# PERFORMANCE OF HARD HANDOFF IN 1xEV-DO REV. A SYSTEMS

A Thesis

by

MAHER AL-SHOUKAIRI

Submitted to the Office of Graduate Studies of
Texas A&M University
in partial fulfillment of the requirements for the degree of

MASTER OF SCIENCE

May 2008

Major Subject: Electrical Engineering

# PERFORMANCE OF HARD HANDOFF IN 1xEV-DO REV. A SYSTEMS

A Thesis

by

MAHER AL-SHOUKAIRI

Submitted to the Office of Graduate Studies of
Texas A&M University
in partial fulfillment of the requirements for the degree of

MASTER OF SCIENCE

Approved by:

| | |
|---|---|
| Co-Chairs of Committee, | Khalid Qaraqe |
| | Erchin Serpedin |
| Committee Members, | Mohamed-Slim Alouini |
| | Narasimha Reddy |
| | Eyad Masad |
| Head of Department, | Costas Georghiades |

May 2008

Major Subject: Electrical Engineering

# ABSTRACT

Performance of Hard Handoff in 1xEV-DO REV. A Systems. (May 2008)

Maher Al-Shoukairi, B.S., University of Jordan, Jordan

Co-Chairs of Advisory Committee: Dr. Khalid Qaraqe
Dr. Erchin Serpedin

1x Evolution-Data Optimized Revision A (1xEV-DO Rev. A) is a cellular communications standard that introduces key enhancements to the high data rate packet switched 1xEV-DO Release 0 standard. The enhancements are driven by the increasing demand on some applications that are delay sensitive and require symmetric data rates on the uplink and the downlink. Some examples of such applications being video telephony and voice over internet protocol (VoIP).

The handoff operation is critical for delay sensitive applications because the mobile station (MS) is not supposed to lose service for long periods of time. Therefore seamless server selection is used in Rev. A systems. This research analyzes the performance of this handoff technique. A theoretical approach is presented to calculate the slot error probability (SEP). The approach enables evaluating the effects of filtering, hysteresis as well as the system introduced delay to handoff execution. Unlike previous works, the model presented in this thesis considers multiple base stations (BS) and accounts for correlation of shadow fading affecting different signal powers received from different BSs. The theoretical results are then verified over ranges of parameters of practical interest using simulations, which are also used to evaluate the packet error rate (PER) and the number of handoffs per second.

Results show that the SEP gives a good indication about the PER. Results also show that when considering practical handoff delays, moderately large filter constants are more efficient than smaller ones.

To My Parents and Brother

# ACKNOWLEDGEMENTS

First and foremost, I would like to express my sincere and heartfelt gratitude to my advisor Dr. Khalid Qaraqe for his guidance, support and patience throughout my study. Working under Dr. Khalid has been a wonderful experience.

I would like to thank Dr. Serpedin for the valuable time and effort he dedicated to help me. I thank Dr. Alouini for being a great source of guidance, help and inspiration. I will always be grateful to Dr. Masad for helping me get this great opportunity, and I thank Dr. Reddy for serving as a member of my graduate committee.

I would also like to thank the Qatar Foundation for Education, Science, and Community Development and Qatar Telecom (Qtel) for funding this research.

I am grateful to all the professors who have taught and motivated me throughout my study at Texas A&M University. I thank all my friends at Jordan and at Texas A&M. Finally, I thank my family for their continuous encouragement and support.

# TABLE OF CONTENTS

# LIST OF FIGURES

# LIST OF TABLES

# CHAPTER I

## INTRODUCTION

As implied by its name the 1xEV-DO is a data optimized (DO) cellular communications standard. It evolved (EV) from previous more established standards to achieve high data rates. The (1x) refers to the fact that 1xEV-DO uses a separate single 1.25 MHz carrier to address only data. The first version of the standard (1xEV-DO Release 0) was originally designed for downlink intensive delay tolerant applications. However, with the increased popularity of high speed wireless Internet access, the demand on applications such as voice over internet protocol (VoIP) and video telephony has increased. In addition to the delay sensitivity of such applications, they also require the system to be able to achieve high data rates on both the uplink and the downlink. Therefore, in order for the 1xEV-DO Release 0 to meet the requirements of the new applications, some enhancements were introduced to the standard in 1xEV-DO Revision A.

One of the key enhancements introduced to meet the latency requirements of some applications is the handoff technique used in Rev. A systems. The system introduces a new channel that is used to provide an early indication in time of the change in the serving base station (BS). The knowledge of the exact time at which the change of serving BS occurs minimizes the transition delay and allows the mobile station (MS) to

_____
This thesis follows the style of *IEEE Transactions on Automatic Control*.

be served by only one BS at all times. However, any delay in the handoff execution will prevent the MS from being served by the BS providing it with the highest received power, causing possible degradation of service quality.

In this research we study the performance of the handoff technique used in Rev. A systems through developing an analytical approach to evaluate the slot error probability (SEP). The novelty of the approach lies in studying the performance while considering the effect of hysteresis, filtering and system introduced delay, and adopting a multiple base station model. This model incorporates a communication channel with Rayleigh and correlated log-normal components. The handoff performance is also studied through packet error rate (PER) and number of handoffs that are both obtained through simulations. This performance study will give some insight into the tradeoff between different system parameters. It will also help in determining suitable values that will achieve best system performance.

The organization of the work is as follows. Chapter II gives a brief description of some of the 1xEV-DO Rev. A system specifications that are needed to understand subsequent chapters. Chapter III presents and explains the channel model used in the analysis. Based on the adopted system model, Chapter IV demonstrates the analytical approach used to evaluate SEP. It also includes model verification using simulations. Chapter V presents simulation results for PER and the handoff rate. Chapter V also includes an explanation of tradeoffs between different system parameters. Finally, Chapter VI offers some conclusions and recommends possible future work.

**CHAPTER II**

**1xEV-DO REV A. OVERVIEW**

**A. Introduction**

Although the main interest of this thesis is the handoff algorithm used on the downlink of 1xEV-DO Rev. A systems, the performance analysis requires a general understanding of the system's data transmission techniques and the channels involved in the process. Moreover understanding the operation of some channels that are directly related to the handoff procedure is necessary for the analysis. Consequently, this chapter briefly discusses data transmission on the downlink of the Rev. A system. It also presents the physical layer channels used on both the uplink and the downlink with specific attention to the data source control (DSC) channel that is essential for the handoff operation. Detailed system specifications can be found in [1] while a good description of the enhancements of 1x EV-DO Rev. A over Release 0 can be found in [2].

**B. Downlink Data Transmission and Physical Layer Channels**

1xEV-DO REV. A systems can support up to 3.072 Mbps peak download and 1.842 Mbps peak upload speeds. To achieve such high rates the system employs techniques such as multi user diversity, hybrid repeat request and receive diversity.

Unless the system needs to meet a delay sensitive application's requirement the access network (AN) would generally transmit data to users who are experiencing good channel conditions with high data rates. The AN waits for users with worse channel conditions to move into a better state, hence it exploits what is known as multi user diversity. Therefore, the forward link uses time division multiplexing (TDM) of code division multiple access (CDMA) signals, where the data of each user is sent during the assigned period of time at a suitable data rate. A 1.667 ms time slot is the basic timing unit in EV-DO systems. As shown in Figure 1, every time slot contains a pilot part, a medium access control (MAC) part and a data part. The data part can carry the traffic or control channel.
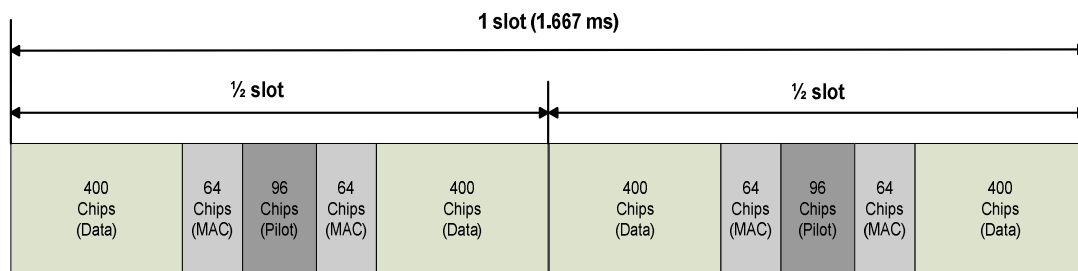


**Fig. 1. The Slot Structure in 1xEV-DO**

Figure 2 shows the downlink channels in Rev A. systems. Every half slot the pilot channel is transmitted for 96 chips at full power providing the MS with 1200 Hz sampling of the communication channel, which is used to estimate the ratio of the received signal power to interference and noise powers (SINR) at the MS. Based on these SINR estimates the MS sends a data rate request to the AN. At the AN a scheduling algorithm designed to efficiently exploit multi user diversity while achieving

fairness between users utilizes these requests to assign data packets for different users at different time slots and different rates.
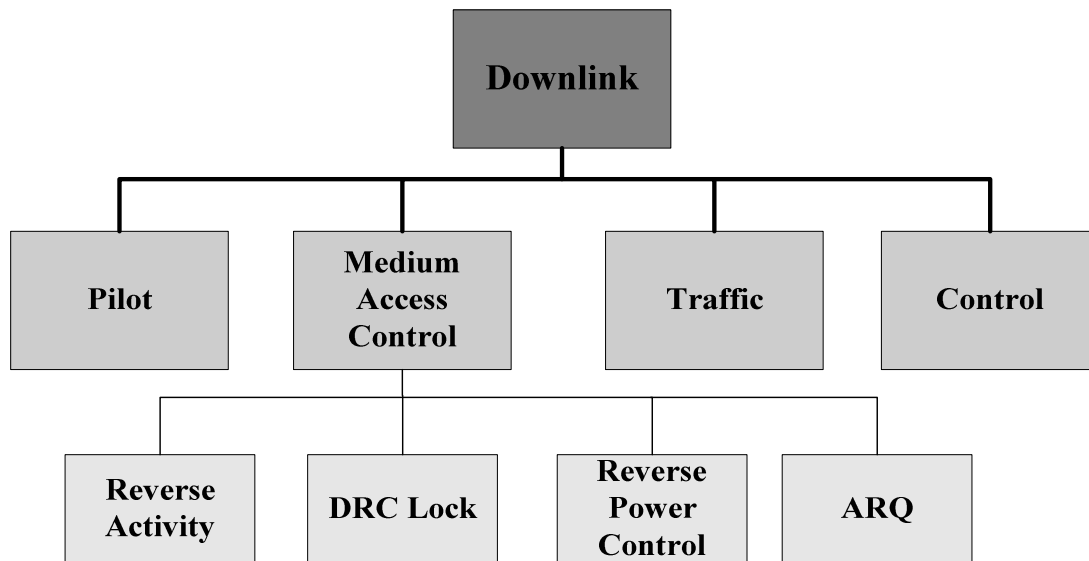


Fig. 2. Physical Layer Downlink Channels

The downlink MAC channel contains four sub-channels:

- Reverse Activity (RA): The network uses the RA channel to transmit the reverse activity bit. The reverse activity bit is used for load control on the reverse link, where it informs the MS to increase or decrease its data rate.

- Data Rate Control (DRC) lock: The DRC lock channel is used to indicate the link quality from the MS to the AN.

- Reverse Power Control (RPC): The RPC channel carries a 1-bit power control command used at the MS for reverse link closed loop power control. It is worth mentioning that power control is only used on the reverse link in EV-DO systems.

- Automatic Repeat Request (ARQ): The ARQ channel is used to inform the MS of whether data packets transmitted on the reverse link were successfully received or not.

The uplink channels are shown in Figure 3. The access channel is used by the MS to begin communications with the network when it does not have an assigned traffic channel. The pilot is used as a reference for coherent detection and timing. On the traffic channel, the auxiliary pilot channel may be used to help decode large packets and the acknowledgment (ACK) channel is used to report to the network if the physical layer packets sent were correctly received at the MS.

The uplink MAC channel consists of the following sub-channels:

- Reverse Rate Indicator (RRI): The RRI channel is used to inform the network of the rate at which the MS packets are being transmitted.

- Data Rate Control (DRC): The DRC channel is used by the MS to indicate to the network the requested data rate on the forward channel. It is also used to indicate the selected serving sector on the downlink through the DRC cover.

- Data Source Control (DSC): In order to minimize handoff delays, the DSC channel is used to provide an indication ahead of time of the change in the serving BS. Due to its importance in the handoff process, the DSC channel will be discussed in more detail in Section E of this chapter.
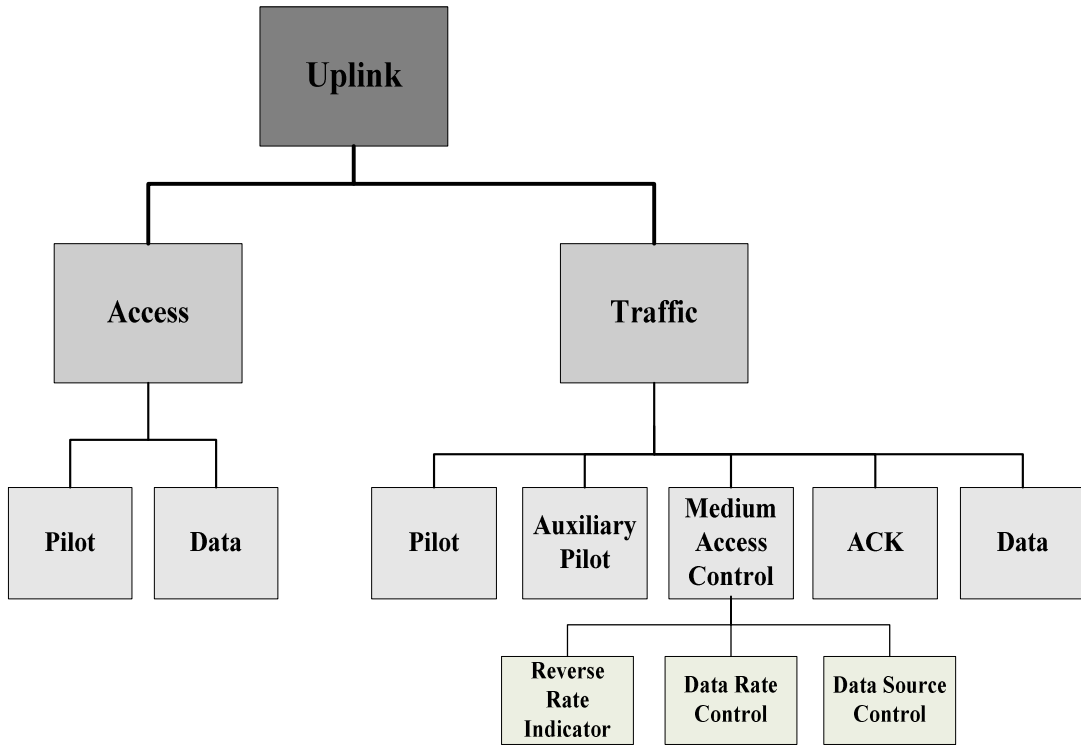
**Fig. 3. Physical Layer Uplink Channels**

## C. Downlink Physical Layer Packet Formats

As mentioned before, data on the forward link is transmitted according to the DRC request made by the MS which is based on forward channel conditions at that time. Therefore physical layer packets can be of different bit lengths with different modulation types and coding rates sent over different slot durations. Table I shows downlink data rates supported by Rev. A systems. The transmission format contains the physical layer packet length in bits, the nominal transmit duration of the packet in slots and the preamble length in chips. The nominal data rate is simply the division outcome of the packet size by the nominal transmission duration in seconds. However as it will be

shown in Section D due to the hybrid automatic repeat request (HARQ) the actual rate could be higher if the MS succeeds in decoding the packet before the maximum number of allowed slots (the nominal transmit duration) is reached. The preamble, which is sent at the beginning of the first slot of a packet is used to identify the intended MS through the MAC index. Since preamble detection is essential for the decoding of a packet, the preamble length is increased in unreliable channel conditions. Consequently, the preamble length is generally inversely proportional to the data rate.

To understand the relation between the values in Table I, an example that uses the highlighted transmission format (1024,2,64) with the nominal data rate of 307.2 kbps is utilized. A packet transmitted with this format carries 1024 data bits with nominal transmit duration of two slots, hence the nominal data rate is

$$Data\ rate = \frac{No.of\ packet\ bits}{Transmit\ duration \times Slot\ period} = \frac{1024}{2 \times 1.667 \times 10^{-3}} = 307.2\ kbps \qquad (2.1)$$

A 1/5 rate code is used to encode the 1024 bits generating 5120 bits to transmit. The modulation type is quadrature phase shift keying (QPSK), therefore every two bits are grouped into one symbol. The number of chips needed to transmit the resulting 2560 symbols is 2560 chips. However, it is shown in Figure 4 that after including the specified preamble in addition to pilot and MAC channels, only 1536 usable data chips are available in the first slot. The rest of the symbols are transmitted in a second slot and the nominal packet duration is two slots.

**Table I**
**Transmission Formats and Data Rates Supported by 1xEV-DO Rev. A**

| Transmission Format<br>(Data bits, Transmit duration, Preamble) | Code Rate | Modulation Type | Nominal Data Rate (kpbs) |
|---|---|---|---|
| (128,16,1024) | 1/5 | QPSK | 4.8 |
| (128,8,512) | 1/5 | QPSK | 9.6 |
| (128,4,1024) | 1/5 | QPSK | 19.2 |
| (128,,4,256) | 1/5 | QPSK | 19.2 |
| (128,2,128) | 1/5 | QPSK | 38.4 |
| (128,1,64) | 1/5 | QPSK | 76.8 |
| (256,16,1024) | 1/5 | QPSK | 9.6 |
| (256,8,512) | 1/5 | QPSK | 19.2 |
| (256,4,1024) | 1/5 | QPSK | 38.4 |
| (256,4,256) | 1/5 | QPSK | 38.4 |
| (256,2,128) | 1/5 | QPSK | 76.8 |
| (256,1,64) | 1/5 | QPSK | 153.6 |
| (512,16,1024) | 1/5 | QPSK | 19.2 |
| (512,8,512) | 1/5 | QPSK | 38.4 |
| (512,4,1024) | 1/5 | QPSK | 76.8 |
| (512,4,256) | 1/5 | QPSK | 76.8 |
| (512,4,128) | 1/5 | QPSK | 76.8 |
| (512,2,128) | 1/5 | QPSK | 153.6 |
| (512,2,64) | 1/5 | QPSK | 153.6 |
| (512,1,64) | 1/5 | QPSK | 307.2 |
| (1024,16,1024) | 1/5 | QPSK | 38.4 |
| (1024,8,512) | 1/5 | QPSK | 76.8 |
| (1024,4,1024) | 1/5 | QPSK | 153.6 |
| (1024,4,256) | 1/5 | QPSK | 153.6 |
| (1024,2,128) | 1/5 | QPSK | 307.2 |
| (1024,2,64) | 1/5 | QPSK | 307.2 |
| (1024,1,64) | 1/3 | QPSK | 614.4 |
| (2048,4,128) | 1/3 | QPSK | 307.2 |
| (2048,2,64) | 1/3 | QPSK | 614.4 |
| (2048,1,64) | 1/3 | QPSK | 1228.8 |
| (3072,2,64) | 1/3 | 8-PSK | 921.6 |
| (3072,1,64) | 1/3 | 8-PSK | 1843.2 |
| (4096,2,64) | 1/3 | 16-QAM | 1228.8 |
| (4096,1,64) | 1/3 | 16-QAM | 2457.6 |
| (5120,2,64) | 1/3 | 16-QAM | 1536.0 |
| (5120,1,64) | 1/3 | 16-QAM | 3072.0 |

**Slot 1**

| 64 Chips (Pre-amble) | 336 Chips (Data) | 64 Chips (MAC) | 96 Chips (Pilot) | 64 Chips (MAC) | 400 Chips (Data) | 400 Chips (Data) | 64 Chips (MAC) | 96 Chips (Pilot) | 64 Chips (MAC) | 400 Chips (Data) |
|---|---|---|---|---|---|---|---|---|---|---|

**Slot 2**

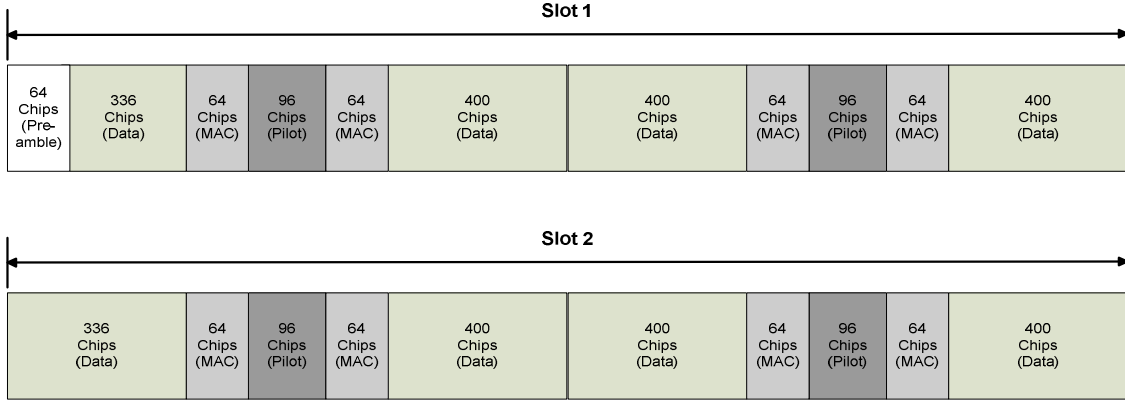| 336 Chips (Data) | 64 Chips (MAC) | 96 Chips (Pilot) | 64 Chips (MAC) | 400 Chips (Data) | 400 Chips (Data) | 64 Chips (MAC) | 96 Chips (Pilot) | 64 Chips (MAC) | 400 Chips (Data) |
|---|---|---|---|---|---|---|---|---|---|

**Fig. 4. Slot Structure of the Transmission Format (1024,2,64)**

## D. Hybrid Automatic Repeat Request

H-ARQ is a technique used to improve the forward link's throughput. The technique is based on dividing each packet into a group of sub-packets, where the data is encoded such that in good channel conditions the receiver would have enough information to decode the data after receiving as little as one sub-packet. However, if it does not succeed, the next sub-packet which carries redundant data will be transmitted increasing the probability of correct decoding of the packet at the receiver. The BS will keep sending sub-packets until the packet is successfully decoded or until all the sub-packets are transmitted. This technique is mostly effective in fast fading conditions, especially when the MS underestimates the downlink channel's quality. Although the MS will be requesting a low data rate packet, there will be a high probability of decoding the packet without the need of transmitting all the sub-packets, which will achieve higher data rates than originally expected by the MS [3].

Figure 5 illustrates how H-ARQ is applied on the downlink of Rev. A systems. Each sub-packet is one slot long and the sub-packets are staggered in time, which means that the sub-packets transmitted for a particular MS are separated by a three slot duration that can be used for transmission of other MS's sub-packets. This time staggering will allow for the MS to try and decode the packet and inform the BS (using the reverse link ACK channel) whether it was successful or not. In Figure 5, a 4-slot packet is transmitted. In case 1, it is assumed that the MS does not succeed in decoding the packet until the reception of the fourth and last sub-packet, consequently the packet is transmitted at the nominal requested data rate. In case 2, however, it is assumed that the MS succeeds in decoding the packet after receiving two sub-packets only, and therefore it achieves double the nominal rate.
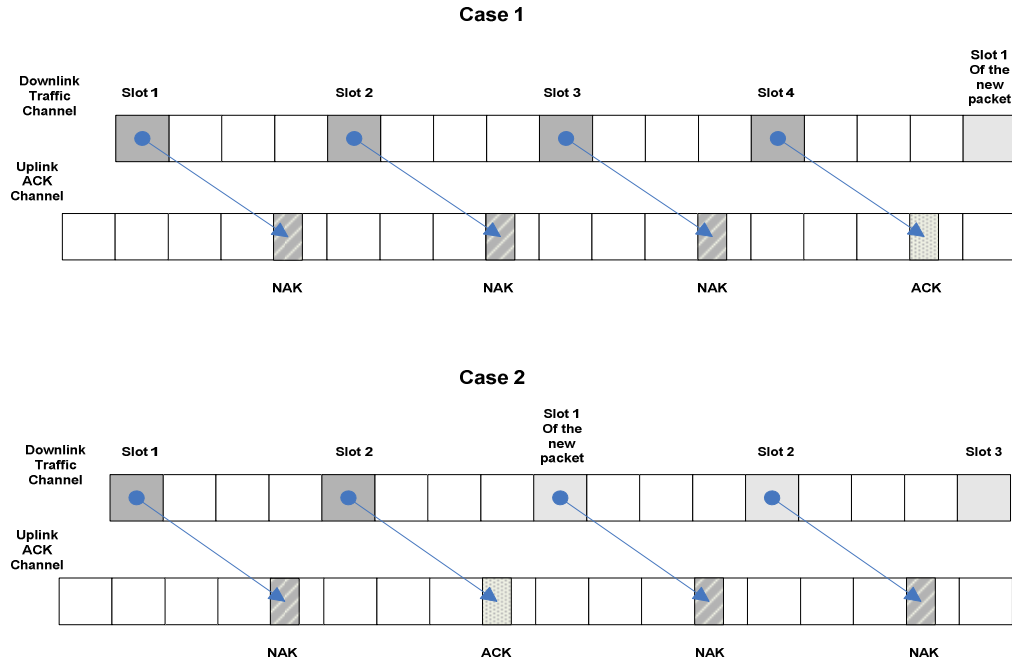
**Fig. 5. H-ARQ Downlink Data Rate Improvement**

**E. Data Source Control (DSC) Channel**

Supporting delay sensitive applications requires a handoff mechanism that would not interrupt the data flow from the BS to the MS. To achieve this the DSC channel was added to Rev. A uplink channels. The DSC channel provides an early indication in time of the change of the serving cell on the downlink. This early indication provides sufficient time for the network to move the data queue from the serving BS to the new one. Therefore at the time of handoff execution the new BS can start serving the MS without any interruption. Since there is no period of time at which the MS is not being served, this operation is referred to as seamless server selection [2].

Figure 6 presents a handoff scenario from BS (A) to BS (B). A DSC cover change can only happen at a DSC boundary. In other words any DSC value is sent for at least one DSC length period. The DSC length is set based on the time needed for the queue to be transferred from one BS to another. Therefore when a handoff decision is made the MS waits for the next DSC boundary to change the DSC cover. Upon the detection of this change by the network it starts transferring the data queue for this specific MS from BS (A) to BS (B). After a DSC length period of time (at the next DSC boundary) the network is expected to have finished the queue transfer, and the DRC cover is changed to point to BS (B), allowing the MS to receive data from the new BS without any interruption [1].

It is worth noting that although there is a time delay between a handoff request and the actual handoff execution, the MS will continue to be served at this period of time

by the second best BS before it switches to the new one. It was found in [4] that due to practical system delays, the actual time between a handoff request and the handoff execution in Rev. A systems is 1.5-2.5 DSC length.
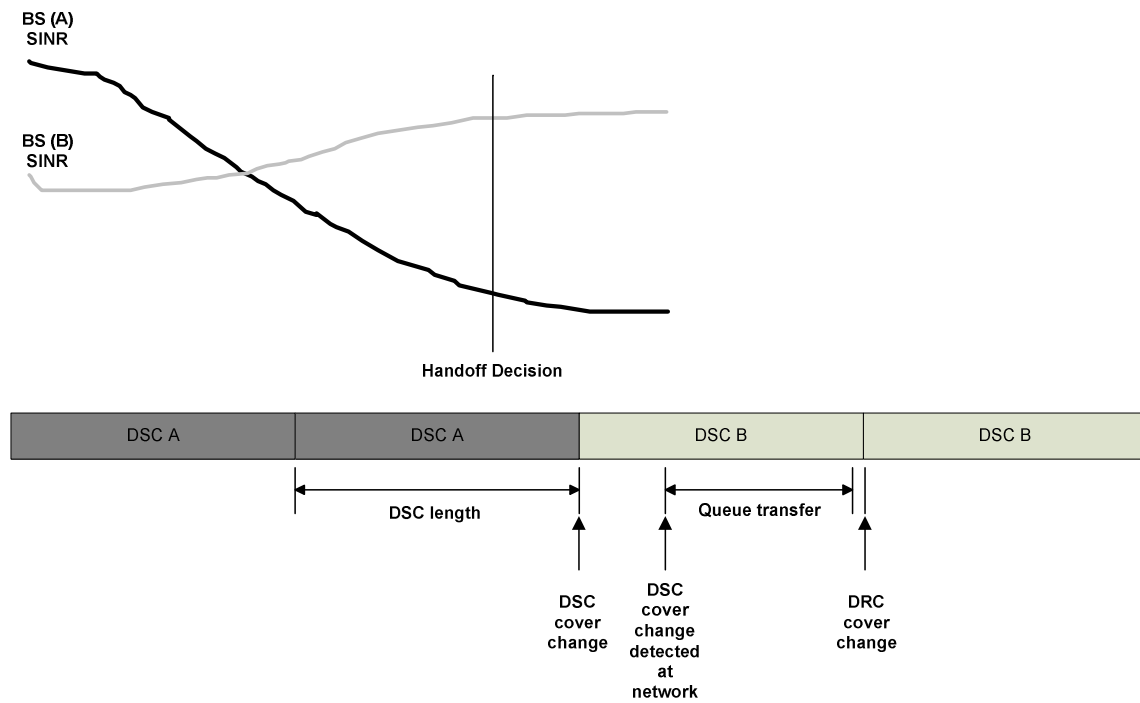
**Fig. 6. A Handoff Scenario Timeline**

# CHAPTER III

## COMMUNICATION CHANNEL MODEL

## A. Introduction

In mobile communications, the MS is expected to move with varying speeds, many of the surrounding objects are randomly and continuously moving as well. Therefore, it is generally very complicated to precisely describe the wireless channel mathematically. However, accurate statistical models have been developed to characterize different phenomena affecting the radio wave propagating through such channels. In cellular systems, the communication channel is usually characterized by path loss, shadow fading and multi-path fading as shown in Figure 7. Additionally for handoff analysis, it is reasonable to consider the case of noiseless interference limited transmission.



**Fig. 7. Combined Path Loss, Shadowing and Multi-path Fading**

**B. Path Loss**

Path loss is caused by the attenuation of the received power per unit area with increasing distance between the transmitter and the receiver in addition to other effects of the propagation channel. Path loss models usu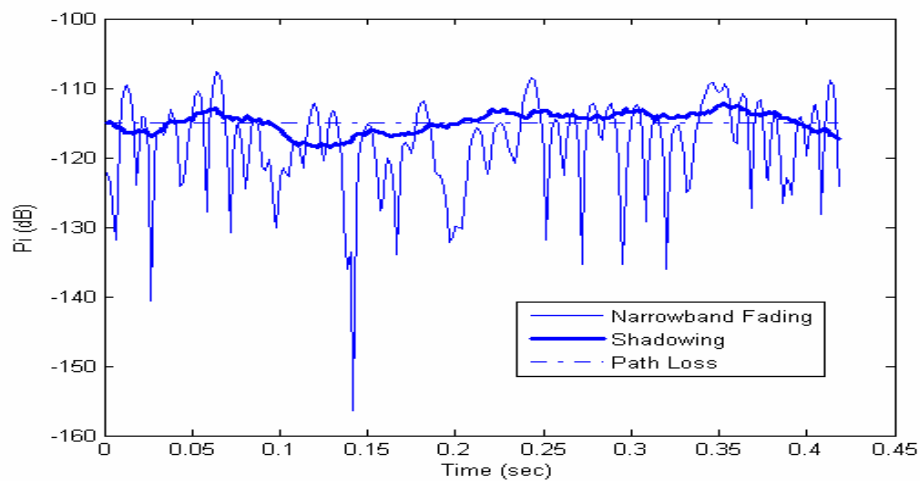ally assume distance dependant attenuation only, which means the power attenuation due to path loss is the same for all points at a given distance from the transmitter.

For our channel model the Okumura model described in [5] was adopted to model the path loss in the dB domain as

$$L_i = K_1 - K_2 \log_{10}(d_i), \tag{3.1}$$

where $d_i$ is the distance between the MS and BS$_i$, $K_1$ is a parameter determined by the transmitter power and $K_2$ is a propagation constant.

**C.    Shadow Fading**

Obstacles between the BS and the MS can cause blockage, absorption, scattering and diffraction of the transmitted signal along different propagation paths. Such effects will cause variations of the received power at the MS. These variations are referred to as shadow fading.

Experimental results show that the shadow fading $W_{l_i}(n)$ can be accurately modeled by a log-normal distribution in the linear domain, resulting in a normal

distribution for $W_i(n)$ in the dB domain. Furthermore, the effects of path loss and shadow fading are often combined to form what is called the large scale propagation effects as follows

$$Y_i(n) = L_i + W_i(n) \tag{3.2}$$

$$Y_{li}(n) = 10^{Y_i(n)/10} \tag{3.3}$$

$$f_{Y_{li}}(y_{li}) = \frac{10}{\sqrt{2\pi} 10 y_{li} \sigma_{Y_i} \ln 10} \exp\left[ -\frac{(10\log_{10} y_{li} - \mu_{Y_i})^2}{2\sigma_{Y_i}^2} \right] \tag{3.4}$$

$$f_{Y_i}(y_i) = \frac{1}{\sqrt{2\pi}\sigma_{Y_i}} \exp\left[ -\frac{(y_i - \mu_{Y_i})^2}{2\sigma_{Y_i}^2} \right], \tag{3.5}$$

where $\mu_{Y_i}$ is the mean of $Y_i$ and is equal to $L_i$, $\sigma_{Y_i}$ is the standard deviation of $Y_i$ in dB typically ranging from 5 to 12 dB with 8.9 dB being the suggested value in [6].

Shadow fading was also found to be correlated over short distances, this spatial correlation was analytically modeled by Gudmundson in [5] to fit empirical measurements.

The model proposes a decaying exponential auto-covariance function as follows

$$C_{Y_iY_i}(\Delta d) = C_{W_iW_i}(\Delta d) = \sigma_{Y_i}^2 \exp[-(|\Delta d| \ln 2)/d_{corr}], \tag{3.6}$$

where $\Delta d$ is the separation between the two points at which the correlation is calculated and $d_{corr}$ is the de-correlation distance typically ranging form 10 to 20m.

In mobile communications, since the receiver is expected to be moving, the spatial correlation translates into a temporal correlation by substituting $v\Delta l T_s$ for $\Delta d$ while $v$ stands for the MS speed and $l$ denotes the time index.

$$C_{Y_iY_i}(l) = \sigma_{Y_i}^{2} \exp[-(vT_s \,|\,l\,|\, \ln 2)/d_{corr}]. \tag{3.7}$$

It is also practical to consider the correlation between different shadow fading components affecting the signals received from different BSs due to the fact that the power received at the MS from different BSs will probably be shadowed by the same obstacles surrounding the MS. A correlation of 50% is suggested in [6].

The shadow fading process is modeled as a first order auto-regressive random process represented by the difference equation

$$W_i(n) = aW_i(n-1) + V_i(n), \tag{3.8}$$

where $V_i(n)$ is a zero-mean stationary white Gaussian noise process with covariance $\sigma_{V_i}^{2}$.

From (3.8) it can be easily shown that

$$E[W_i(n)W_i(n-l)] = C_{Y_iY_i}(l) = \sigma_{Vi}^{2} \frac{a^{|l|}}{1-a^{2}}. \tag{3.9}$$

By comparing (3.7) and (3.9), $a$ and $\sigma_{Vi}^{2}$ are determined as

$$a = \exp(-(vT_s \ln 2)/d_{corr}), \ \sigma_{V_i}^{2} = (1-a^{2})\sigma_{Y_i}^{2}. \tag{3.10}$$

Figure 8 shows a comparison between the theoretical auto-covariance of a shadow fading process and that of a simulated process using the results above.
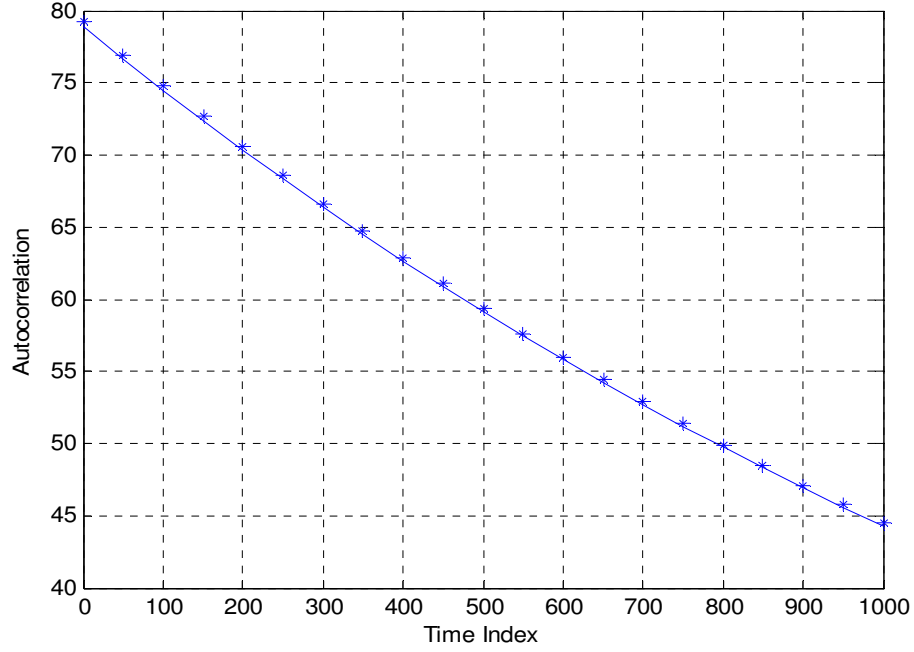
**Fig. 8. Auto-Covariance of the Simulated Shadowing Against Theoretical Auto-Covariance**

## D. Multi-path Fading

Due to reflections from the ground and surrounding structures, the received signal at the MS from any BS will be a combination of several versions of the transmitted signal received at different delays as shown in Figure 9. The constructive and destructive addition of these different versions will cause rapid fluctuation of the amplitude of the received signal over a short period of time or distance. This is referred to as the multi-path or small scale fading. Another phenomenon experienced at the MS due to its movement is the Doppler frequency shift. Since the movement of the MS over a short period of time $\Delta t$ will force the received signal to travel an extra distance of

$\Delta d = v\Delta t \cos(\theta)$ where $\theta$ is the arrival angle of the received signal relative to the direction of motion. This will cause a phase change in the received signal which can be translated into a frequency change of $f_D = v\cos(\theta)/\lambda$ where $\lambda$ is the signal wavelength.
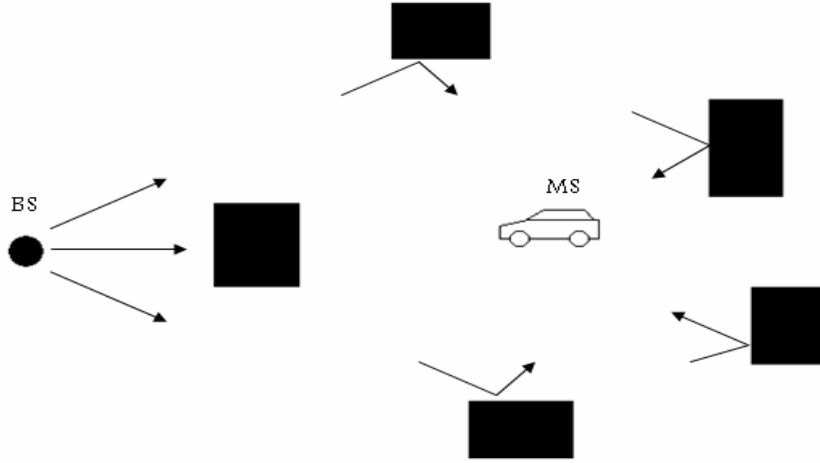
**Fig. 9. Reflected Versions of the Transmitted Signal in a Scattering Environment**

The delay spread is defined as the delay in reception between the first and last significant versions of the transmitted signal. Based on the amount of delay spread in relevance to the inverse bandwidth of the signal itself, multi-path fading can be classified in two different types: narrowband fading and wideband fading. In narrowband fading, the delay spread is small relative to the inverse signal bandwidth causing all the multi-path components to be nonresolvable. While in wideband fading the delay spread is large causing the multi-path components to be resolvable. In this analysis, narrowband fading described by the Clarke's model [7] is adopted. Let the transmitted signal be

$$s(t) = \Re\{u(t)e^{j2\pi f_c t}\},$$
(3.11)

where $u(t)$ is the complex envelope of $x(t)$ and $f_c$ is the carrier frequency. Assuming $N$ reflected versions of the original signal were received at the MS, each version with a delay $\tau_n$ and an attenuation of $\alpha_n$ and considering the phase change due to the delay as well as the Doppler frequency shift, the received signal can be written as

$$y(t) = \Re\left\{e^{j2\pi f_c t}\left(\sum_{n=0}^{N} u(t-\tau_n)\alpha_n e^{-j(2\pi f_c \tau_n + \phi_{D_n})}\right)\right\},$$
(3.12)

where $\tau_n$ is the delay associated with the path $n$ and $\phi_{D_n}$ is the Doppler phase shift and is equal to $\int_{\tau_n} 2\pi f_{D_n}(t)dt$. Since the delay spread is assumed to be small relative to the inverse signal bandwidth, it is reasonable to assume that $u(t)$ does not change over different paths with different delays i.e. $u(t-\tau_n) = u(t)$,

$$y(t) = y_I(t)u(t)\cos(2\pi f_c t) + y_Q(t)u(t)\cos(2\pi f_c t)$$
(3.13)

$$y_I(t) = \sum_{n=0}^{N} \alpha_n \cos(-j2\pi f_c \tau_n + \phi_{D_n})$$
(3.14)

$$y_Q(t) = \sum_{n=0}^{N} \alpha_n \sin(-j2\pi f_c \tau_n + \phi_{D_n}).$$
(3.15)

In a dense scattering environment where $N$ is large the central limit theorem can be invoked to approximate $y_I(t)$ and $y_Q(t)$ as jointly Gaussian random processes. Therefore $X(t) = \sqrt{y_I(t)^2 + y_Q(t)^2}$ will be a Rayleigh distributed random process. The

Clarke's model also defines the temporal properties of this process with its auto-covariance

$$C_{X_i^2 X_i^2}(\tau) = J_o^{\ 2}(2\pi f_d \tau), \tag{3.16}$$

which is expressed in the discrete time domain as

$$C_{X_i^2 X_i^2}(l) = J_o^{\ 2}(2\pi f_d T_s l), \tag{3.17}$$

where $J_o(x)$ is the zeroth order Bessel function of the first kind and $f_d$ is the maximum Doppler frequency.

The Rayleigh fading process can be simulated using several techniques. The sum of sinusoids technique described in [8] was used for the simulations in the following chapters. A comparison between the auto-covariance of the theoretical and simulated processes is shown in Figure 10.
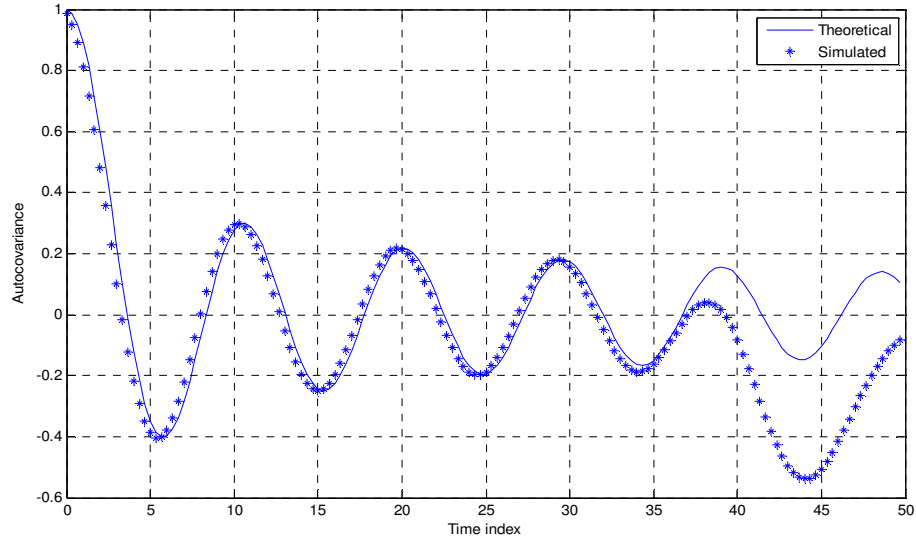


**Fig. 10. Auto-Covariance of the Simulated Rayleigh Process Against Theoretical Bessel Auto-Covariance**

# CHAPTER IV

## HANDOFF PERFORMANCE – SLOT ERROR PROBABILITY

### A. Introduction

This chapter includes an analytical approach to study the performance of the handoff algorithm in 1xEV-DO REV. A systems through the slot error probability. The approach is based on a simplified performance model usually used for system simulations. This simplification is necessary since in REV. A systems the downlink transfer rates are high (up to 3.072 Mbps) which makes link level simulations employing symbol level detection and turbo coding computationally intensive. As an alternate solution slot simulations are used. For every slot period, the signal to interference and noise ratio (SINR) is determined and then compared to a threshold to decide whether an error has occurred.

The analytical approach is also verified using SEP simulations over parameters of practical interest.

### B. System Model and the Handoff Algorithm

The MS is assumed to be at equal distance from four base stations as shown in Figure 11. At any point of time the MS will be connected to one of the four BSs, while

the rest are considered to be interferers. Based on the channel model presented in Chapter III, the power of the signal received from BS$_i$ (in decibels) is

$$P_i = Y_i(n) + 10\log_{10}(X_i(n)^2),\qquad(4.1)$$

where $Y_i(n)$ represents the combined path loss and shadow fading components and $X_i(n)$ represents the Rayleigh fading component.
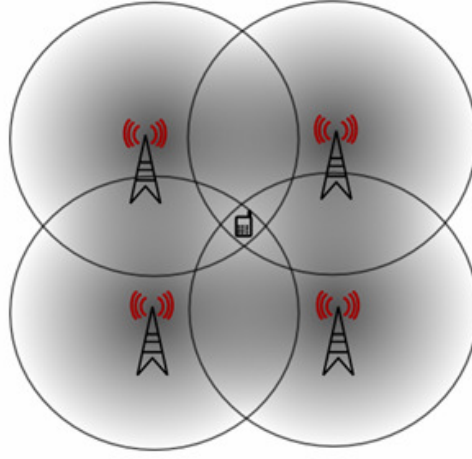


**Fig. 11. The Four Cell Model**

The MS should be generally connected to the BS that will provide the highest signal to interference power ratio to achieve best performance. However, to avoid unnecessary handoffs resulting from the rapid signal changes imposed by the Rayleigh fading, the received signal to interference ration (SIR) is filtered, allowing for better tracking of the average signal strength. Furthermore, the algorithm requires the filtered SIR from BS$_i$ to exceed the one from BS$_j$ by a specified hysteresis before initiating a

handoff from $BS_j$ to $BS_i$. The hysteresis will protect the system from rapid continuous handoffs between the BSs, which is known as the ping-pong effect.

The SIR at the MS when it is being served by $BS_i$ is

$$S_i(n) = P_i(n) - P_{\Sigma i}(n),$$ (4.2)

where $P_{\Sigma i}(n) = 10\log_{10}(\sum_{j \neq i}^{N} 10^{P_j(n)/10})$. The filtered SIR is given by

$$F_i(n) = S_i(n) * h(n),$$ (4.3)

where $h(n)$ is the filter's impulse response and $*$ denotes linear convolution. The handoff request can then be written as

$$
\begin{aligned}
R(n) \quad &= 1 & F_1(n) - F_{\max_1}(n) \geq H \\
&= 2 & F_2(n) - F_{\max_2}(n) \geq H \\
&= 3 & F_3(n) - F_{\max_3}(n) \geq H \\
&= 4 & F_4(n) - F_{\max_4}(n) \geq H \\
&= R(n-1) & otherwise \quad ,
\end{aligned}
$$ (4.4)

where $F_{\max_i}(n)$ is $\max_{j \neq i}[F_j(n)]$ and $R(n) = i$ is the request at time n to connect to $BS_i$.

## C. Slot Error Probability Evaluation

By definition a slot error is assumed to occur if the received SIR drops below a specified threshold (T). This means that a slot error occurs if $BS_i$ is serving the MS and $S_i(n) < T$.

$$SEP = \sum_i \int_{-\infty}^{T} f(S_i(n), C(n) = i)dS_i,$$ (4.5)

where $f(S_i(n), C(n) = i)$ is the joint probability density function of $S_i(n)$ and $C(n)=i$ denotes that the MS is being served by $BS_i$ at time i. $C(n)$ is introduced to compensate for the delay $k$ introduced by the system between a handoff request $R(n-k)$ and the connection based on that request $C(n)$. As mentioned in Chapter II this delay was found in [4] to be 1.5- 2.5 (DSClength). To evaluate (4.5) we follow the approach in [9] and [4]. Defining

$$FS_i = F_i - F_{\max_i},\tag{4.6}$$

and changing the representation of the time indices to subscripts

$$f(S_{i_n}, C_n = i) = f(S_{i_n}, R_{n-k} = i) = \int_{-\infty}^{\infty} f(S_{i_n}, R_{n-k} = 1 \mid FS_{i(n-k)}) f(FS_{i(n-k)}) dFS_{i(n-k)} \tag{4.7}$$

$$f(S_{i_n}, R_{n-k} = 1 \mid FS_{i(n-k)}) = \begin{cases} f(S_{i_n} \mid FS_{i(n-k)}) & FS_{i(n-k)} \geq H \\ 0 & FS_{i(n-k)} \leq -H \end{cases} \tag{4.8}$$

$$f(S_{i_n}, R_{n-k} = 1 \mid FS_{i(n-k)}) = \gamma f(S_{i_n} \mid FS_{i(n-k)}) \quad \mid FS_{i(n-k)} \mid \leq H, \tag{4.9}$$

where $\gamma$ is the probability of ($\mid FS_{i(n-k)} \mid \leq H$ and $C_n = i$ ). Knowing that the MS will always be served by $BS_i$ when $F_i$ is greater than all the other received SIRs by at least the hysteresis value H, and $\gamma$ is the percentage of the time when $F_i$ is within –H to H from the second best SIR, $\gamma$ can be evaluated by

$$P(C_n = i) = P(FS_i > H) + \gamma P(\mid FS_i \mid < H) \tag{4.10}$$

$$P(C_n = i) = \int\limits_{H}^{\infty} f(FS_i)dFS_i + \gamma \int\limits_{-H}^{H} f(FS_i)dFS_i$$

$$\gamma = \frac{P(C_n = i) - \int\limits_{H}^{\infty} f(FS_i)dFS_i}{\int\limits_{-H}^{H} f(FS_i)dFS_i}, \tag{4.11}$$

Moreover since the MS is at equal distance from all BSs and since all $P_i$'s are identically distributed, $P(C_n = i)$ is equal to 0.25.

The joint distribution of $S_{in}$ and $C_n = i$ is

$$f(S_{in}, C_n = i) = \int\limits_{H}^{\infty} f(S_{in}, FS_{i(n-k)})dFS_{i(n-k)} + \gamma \int\limits_{-H}^{H} f(S_{in}, FS_{i(n-k)})dFS_{i(n-k)}. \tag{4.12}$$

Therefore the slot error probability is given by

$$SEP = 4(\int\limits_{-\infty}^{T}\int\limits_{H}^{\infty} f(S_i(n), FS_{i(n-k)})dFS_{i(n-k)}dS_i + \gamma \int\limits_{-\infty}^{T}\int\limits_{-H}^{H} f(S_i(n), FS_{i(n-k)})dFS_{i(n-k)}dS_i). \tag{4.13}$$

To evaluate (4.13) some approximations are made to keep the analysis tractable.

### 1. Received Power Statistics

The received power at the MS from any of the serving BSs is a product of a Rayleigh process and a lognormal process. The distribution of the received power is therefore a composite Rayleigh-lognormal distribution. This distribution is mathematically intractable, however some alternative distributions can be used to efficiently approximate it. Over certain ranges of lognormal standard deviation ($\sigma_{Y_i} > 6$

dB) it is generally acceptable to use a lognormal distribution to approximate the composite distribution. Since typical shadow standard deviation values range from 5 to 12 dB (with 8.9 dB suggested by the 3rd generation partnership project 2 (3GPP2) in [6]) we can assume the distribution of received power $P_i$ to be lognormal. The mean and standard deviation of the new lognormal were found in [10] by calculating the mean and standard deviation of the Susuki distribution which models the probability density function of the composite distribution.

$$f(P_{li}) = \int_0^\infty \frac{1}{\eta} e^{-P_{li}/\eta} \frac{1}{\lambda\sqrt{2\pi}\sigma_{Y_i}\eta} \exp\left\{\frac{-(\ln\eta/\lambda - \ln\mu_{Y_i}/\lambda)^2}{2\sigma_{Yi}^2}\right\} d\eta, \qquad (4.14)$$

where $\lambda = \ln(10)/10$ and $P_{li} = 10^{P_i/10}$.

$$E[P_i] = \int_0^\infty 10\log_{10}(P_{li}) f(P_{li}) dP_{li}, \qquad (4.15)$$

$$E[P_i^2] = \int_0^\infty (10\log_{10}(P_{li}))^2 f(P_{li}) dP_{li}. \qquad (4.16)$$

Equations (4.15) and (4.16) were solved in [10] to find the new mean and standard deviation as follows

$$\mu_{Pi} = \mu_{Yi} - 2.5\,dB, \qquad (4.17)$$

$$\sigma_{Pi} = \sqrt{\sigma_{Yi}^2 + 5.57^2}, \qquad (4.18)$$

The correlation between the different powers received from different base stations can be found by using equations from [11]

$$\rho_{P_iP_j} = \frac{\ln(1+\frac{\mathrm{cov}[P_{li},P_{lj}]}{M_{P_{li}}M_{P_{lj}}})}{\lambda^2\sigma_{P_i}\sigma_{P_j}} \tag{4.19}$$

$$M_{P_{li}} = M_{Y_{li}} = \exp(\lambda M_{Y_i} + \frac{\lambda^2}{2}\sigma_{Y_i}{}^2), \tag{4.20}$$

where $\lambda = \ln(10)/10$, $P_{li} = 10^{P_i/10}$, $M_{Y_i}$ and $\sigma_{Y_i}$ are the mean and standard deviation of $Y_i$,

respectively, $M_{P_{li}}$ and $\sigma_{P_{li}}$ are the mean and standard deviation of $P_{li}$, respectively.

$$\mathrm{cov}[P_{li},P_{lj}] = (\rho_{Y_iY_j}\sigma_{Y_{li}}\sigma_{Y_{lj}} + M_{Y_{li}}M_{Y_{lj}})E[X_i{}^2X_j{}^2] - M_{Y_{li}}M_{Y_{lj}} \tag{4.21}$$

$$\rho_{Y_{li}Y_{lj}} = \frac{\exp(\lambda^2\rho_{Y_iY_j}\sigma_{Y_i}\sigma_{Y_j})-1}{(\exp(\lambda^2\sigma_{Y_i}{}^2)-1)(\exp(\lambda^2\sigma_{Y_j}{}^2)-1)} \tag{4.22}$$

$$\sigma_{Y_{li}}{}^2 = \exp(2\lambda M_{Y_i} + \lambda^2\sigma_{Y_i}{}^2)(\exp(\lambda^2\sigma_{Y_i}{}^2)-1), \tag{4.23}$$

where $Y_{li} = 10^{Y_i/10}$, $M_{Y_{li}}$ is the mean of $Y_{li}$ and $\sigma_{Y_{li}}$ is the standard deviation of $Y_{li}$.

## 2. Signal to Interference Ratio Statistics

The signal to interference ratio (SIR) is defined in (4.2) as $S_i(n) = P_i(n) - P_{\Sigma i}(n)$.

Therefore, to find $S_i(n)$'s distribution we need to find the distribution of $P_{\Sigma i}(n)$, where

$P_{\Sigma i}(n)$ is the linear summation of a group of lognormals. This problem of finding the

distribution of the sum of a group of lognormals has been extensively studied due to its

importance in the analysis of interference in wireless and especially cellular systems. A

simple yet a good solution assumes the distribution of the sum of the lognormals to be

also lognormal. Based on this assumption the Schwartz and Yeh's method [12] evaluates the mean and standard deviation of the new lognormal by matching them to those of the sum in the dB domain. The method starts by finding a numerical solution for the mean and standard deviation for the sum of only two lognormals. Then based on the assumption that the new distribution is also lognormal the procedure is repeated to find the new mean and standard deviation as follows,

$$Q_i = \ln P_{li} = \lambda P_i \tag{4.24}$$

$$\mu_{Q_i} = \lambda \mu_{P_i}, \quad \sigma_{Q_i} = \lambda \sigma_{P_i}, \tag{4.25}$$

where $Q_i$ is introduced to simplify the analysis.

$$Q_{\Sigma i} = \ln(\sum_{j \neq i} e^{Q_j}) \tag{4.26}$$

$$Q_{j,k} = \ln(e^{Q_j} + e^{Q_k}) \tag{4.27}$$

$$E[Q_{j,k}] = \mu_{Q_{j,k}} = E[\ln(e^{Q_j} + e^{Q_k})] \tag{4.28}$$

$$E[Q_{j,k}{}^2] = \mu_{Q_{j,k}}^2 + \sigma_{Q_{j,k}}^2 = E[\ln^2(e^{Q_j} + e^{Q_k})] \tag{4.29}$$

Rearranging equation (4.28)

$$\begin{aligned}
\mu_{Q_{j,k}} &= E[\ln(e^{Q_j})] + E[\ln(1 + \frac{e^{Q_k}}{e^{Q_j}})] \\
&= \mu_{Q_j} + E[\ln(1 + \frac{e^{Q_k}}{e^{Q_j}})] ,
\end{aligned} \tag{4.30}$$

where $E[\ln(1 + \frac{e^{Q_k}}{e^{Q_j}})]$ is calculated numerically keeping in mind that $\frac{e^{Q_k}}{e^{Q_j}}$ is also lognormal. Using the same approach $\sigma_{Q_{j,k}}^2$ is evaluated.

Applying this approach recursively and taking into consideration the correlation between different lognormals, [13] shows how to find the mean and standard deviation. Starting with

$$Z_1 = Q_1,$$ (4.31)

and defining

$$Z = Q_{\Sigma i}, \; Z_k = \ln(e^{Z_{k-1}} + e^{Q_k}), \; \rho_{Q_i Q_j} = \rho_{P_i P_j},$$ (4.32)

we have

$$\mu_{Z_k} = \mu_{Z_{k-1}} + G_1(\mu_{w_k}, \sigma_{w_k})$$ (4.33)

$$\sigma_{Z_k}{}^2 = \sigma^2{}_{Z_{k-1}} - G_1{}^2(\mu_{w_k}, \sigma_{w_k}) + G_2(\mu_{w_k}, \sigma_{w_k}) - 2\frac{(\rho_{(Z_{k-1})(Q_k)}\sigma_{Q_k} - \sigma_{Z_{k-1}})\sigma_{Z_{k-1}}}{\sigma^2{}_{w_k}} G_3(\mu_{w_k}, \sigma_{w_k})$$ (4.34)

$$\rho_{(Z_{k-1})(Q_k)} = \sigma_{Z_{k-2}} \frac{\rho_{(Zk-2)(Q_k)}}{\sigma_{z_{k-1}}} + \frac{\rho_{(Q_{k-1})(Q_k)}\sigma_{Q_{k-1}} - \rho_{(Z_{k-2})(Qk)}\sigma_{Z_{k-2}}}{\sigma_{Z_{k-1}}\sigma^2_{w_{k-1}}} G_3(\mu_{w_{k-1}}, \sigma_{w_{k-1}}),$$ (4.35)

where $\mu_{w_k}$ and $\sigma_{w_k}$ are the mean and standard deviation of

$$w_k = Q_k - Z_{k-1},$$ (4.36)

and are equal to

$$\mu_{w_k} = \mu_{Qk} - \mu_{Z_{k-1}}$$ (4.37)

$$\sigma_{w_k} = \sqrt{\sigma_{Q_k}^2 + \sigma_{Z_{k-1}}^2} \; .$$ (4.38)

$G_1$, $G_2$ and $G_3$ are evaluated numerically and are given by

$$G_1(\mu_{w_k}, \sigma_{w_k}) = E\{\ln(1 + e^{w_k})\}$$ (4.39)

$$G_2(\mu_{w_k}, \sigma_{w_k}) = E\{\ln^2(1 + e^{w_k})\}$$ (4.40)

$$G_3(\mu_{w_k}, \sigma_{w_k}) = E\{(w_k - \mu_{w_k})\ln(1 + e^{w_k})\}. \tag{4.41}$$

Finally

$$\mu_{P_{\Sigma i}} = \mu_{Z_N}/\lambda, \ \sigma_{P_{\Sigma i}} = \sigma_{Z_N}/\lambda. \tag{4.42}$$

Since both $P_i(n)$ and $P_{\Sigma i}(n)$ are assumed to be normally distributed, the outcome of the subtraction of $P_{\Sigma i}(n)$ from $P_i(n)$ is normally distributed as well with mean and standard deviation given repectively by

$$M_{S_i} = M_{Y_i} - M_{P_{\Sigma i}}, \ \sigma_{S_i}^{\ 2} = \sigma_{P_i}^{\ 2} + \sigma_{P_{\Sigma i}}^{\ 2} - 2\rho_{P_i P_{\Sigma i}} \sigma_{P_i} \sigma_{P_{\Sigma i}}. \tag{4.43}$$

The correlation between different SIRs can be found using an approach similar to that presented in [14]. In general, the correlation between different sums of lognormals can be calculated as follows

$$A = 10\log_{10}(10^{P_1/10} + 10^{P_2/10}.....10^{P_N/10})$$
$$B = 10\log_{10}(10^{P_1/10} + 10^{P_2/10}.....10^{P_M/10})$$
$$E[10^{A/10}10^{B/10}] = E[(10^{P_1/10} + 10^{P_2/10}.....10^{P_N/10})(10^{P_1/10} + 10^{P_2/10}.....10^{P_M/10})]$$

$$= \sum_{i=1}^{N}\sum_{j=1}^{M} E[10^{(P_i+P_j)/10}] = \sum_{i=1}^{N}\sum_{j=1}^{M} e^{\lambda M_{P_i} + \lambda M_{P_j} + \frac{1}{2}\lambda^2(\sigma_{P_i}^2 + \sigma_{P_j}^2 + 2\rho_{P_i P_j}\sigma_{P_i}\sigma_{P_j})}. \tag{4.44}$$

Then again from [11]

$$\rho_{AB} = \frac{\ln(1 + \dfrac{E[10^{A/10}10^{B/10}]}{M_A M_B})}{\lambda^2 \sigma_A \sigma_B}. \tag{4.45}$$

An extension to Wilkinson's approach is used to find the auto and cross-covariance functions between different SIRs. The approach is based on matching the

auto-covariance function of the new process to that of the summation of the lognormals in the linear domain and then transferring it back to the dB domain.

The cross-covariance between two correlated shadow fading processes was found in [15]

$$C_{Y_i Y_j}(l) = \rho_{Y_i Y_j} C_{Y_i Y_i}(l), \tag{4.46}$$

and the auto-covariance of the Rayleigh fading process $X_i$ is given by

$$R_{X_i^2}(l) = E[X_i^2(n)X_i^2(n+l)] = Jo^2(2\pi f_d T_s l) + 1. \tag{4.47}$$

Therefore the auto-correlation function between two shadow fading processes in the linear domain is [16]

$$R_{Y_{li}Y_{lj}}(l) = E[10^{Yi(n)/10}10^{Yj(n+l)/10}] = \exp(\lambda(M_{Y_i} + M_{Y_j}) + \frac{1}{2}\lambda^2(\sigma_{Y_i}^2 + \sigma_{Y_j}^2) + C_{Y_iY_j}(l)), \tag{4.48}$$

and the auto-correlation function between the power received from BS$_i$ and the power received from BS$_j$ in the linear domain is

$$
\begin{aligned}
R_{P_{li}P_{lj}}(l) &= R_{X_i^2 X_j^2}(l)E[10^{P_i(n)/10}10^{P_j(n+l)/10}] \\
&= R_{X_i^2 X_j^2}(l)\exp(\lambda(M_{Y_i} + M_{Y_j}) + \frac{1}{2}\lambda^2(\sigma_{Y_i}^2 + \sigma_{Y_j}^2) + C_{Y_iY_j}(l)),
\end{aligned} \tag{4.49}
$$

where $P_{li} = X_i^2 Y_{li}$. Again in general if

$$
\begin{aligned}
A &= 10\log_{10}(10^{P_1/10} + 10^{P_2/10}.....10^{P_N/10}) \\
B &= 10\log_{10}(10^{P_1/10} + 10^{P_2/10}.....10^{P_M/10})
\end{aligned}
$$

then

$$E[10^{A(n)/10}10^{B(n+l)/10}]$$

$$= E[(10^{P_1(n)/10} + 10^{P_2(n)/10}.....10^{P_N(n)/10})(10^{P_1(n+l)/10} + 10^{P_2(n+l)/10}.....10^{P_M(n+l)/10})] \quad (4.50)$$

$$= \sum_{i=1}^{N} \sum_{j=1}^{M} R_{X_i^2 X_j^2}(l) e^{\lambda(M_{Y_i} + M_{Y_j}) + \frac{1}{2}\lambda^2(\sigma_{Y_i}^2 + \sigma_{Y_j}^2) + C_{Y_i Y_j}(l)}$$

$$C_{AB}(l) = (\ln(E[10^{A(n)/10}10^{B(n+l)/10}]) - \lambda M_A M_B - \frac{1}{2}\lambda^2(\sigma_A^2 + \sigma_B^2))/\lambda^2. \quad (4.51)$$

The auto-covariance function between any two SIRs is

$$C_{S_i S_j}(l) = E[(P_i(n) - P_{\Sigma i}(n))(P_j(n+l) - P_{\Sigma j}(n+l))]$$

$$= E[P_i(n)P_j(n+l)] - E[P_i(n)P_{\Sigma j}(n+l)] - E[P_{\Sigma i}(n)P_j(n+l)] + E[P_{\Sigma i}(n)P_{\Sigma j}(n+l)]$$

$$= C_{PiPj}(l) - C_{PiP_{\Sigma j}}(l) - C_{P_{\Sigma i}P_j}(l) + C_{P_{\Sigma i}P_{\Sigma j}}(l), \quad (4.52)$$

where the covariance functions in (4.52) are evaluated using (4.51).

## 3. Filtered SIRs Statistics

The filter used to eliminate the fast Rayleigh fading variations is typically a first order IIR low pass filter [9]. The impulse response of the filter was chosen in [4] to be

$$h(n) = (1/T_{iir})(1 - 1/T_{iir})^n. \quad (4.53)$$

Since the filter is linear the filtered SIRs will also be normally distributed with mean

$$\mu_{F_i} = E[F_i] = \mu_{S_i}. \quad (4.54)$$

The auto and cross-covariance functions between filtered SIRs and filtered and unfiltered SIR's are

$$C_{F_i S_j}(l) = [h(l) * S_i(l)] * S_j(-l) = h(l) * [S_i(l) * S_j(-l)] = h(l) * C_{S_i S_j}(l) = C_{S_i F_j}(l) \quad (4.55)$$

$$C_{F_i F_j}(l) = [h(l) * S_i(l)] * [h(-l) * S_j(-l)] = h(l) * h(-l) * C_{S_i S_j}(l), \quad (4.56)$$

where $h(l)*h(-l)=(1/T_{iir})(1-1/T_{iir})^{|l|}$ [17]. Standard deviations of the filtered SIRs

along with different correlation coefficients can be found using the filtered auto and

cross-covariance functions

$$\sigma_{F_i}=C_{F_iF_i}(0) \tag{4.57}$$

$$\rho_{F_iF_j}=C_{F_iF_j}(0)/(\sigma_{F_i}\sigma_{F_j}) \tag{4.58}$$

$$\rho_{S_iF_{j(n-k)}}=C_{F_iS_j}(-k)/(\sigma_{S_i}\sigma_{F_j}). \tag{4.59}$$

## 4. The Maximum of a Group of Filtered SIRs

As mentioned before when the MS is being served by $BS_i$, a handoff operation

will only be initiated if the received SIR from any other BS ($F_j$) is greater than the

current filtered SIR $F_i$ by the heteresis value H. In other words, if the maximum of the

three filtered SIRs ($F_{max_i}$) exceeds the current filtered SIR by H, then the MS initiates a

handoff request. Therefore finding the distribution of the maximum of the three

remaining filtered SIRs is essential for the analysis of the handoff performance. Since in

the previous sections the filtered SIRs were approximated by normal distributions, the

Clark's approach can be used to find the distribution of their maximum. The approach

starts by matching the moments of a new normal distribution to that of the maximum of

only two. The same procedure is then repeated using a pair at a time. Clearly the

approximation is more accurate for the case of a small number of random processes

(three in this case), since the assumption of the maximum being normally distributed

becomes less accurate as the number of random processes increases. The approach starts

by defining

$$\phi(x) = \frac{1}{\sqrt{2\pi}} \exp(-\frac{x^2}{2}) \tag{4.60}$$

$$\Phi(y) = \int_{-\infty}^{y} \phi(x) dx \tag{4.61}$$

$$a = (\sigma_{F_l}^2 + \sigma_{F_j}^2 - 2\rho_{F_l F_j} \sigma_{F_l} \sigma_{F_j})^{.5} \tag{4.62}$$

$$\alpha = \frac{\mu_{F_l} - \mu_{F_j}}{a} \ . \tag{4.63}$$

Then for $F_{\max l,j} = \max(F_l, F_j)$ the mean and the variance are

$$\mu_{F_{\max l,j}} = \mu_{Fl}\Phi(\alpha) + \mu_{Fj}\Phi(-\alpha) + a\phi(\alpha) \tag{4.64}$$

$$\sigma_{F_{\max l,j}}^2 = (\sigma_{Fl}^2 + \mu_{Fj}^2)\Phi(\alpha) + (\sigma_{Fl}^2 + \mu_{Fj}^2)\Phi(-\alpha) + (\mu_{Fl} + \mu_{Fj})a\phi(\alpha) - \mu_{F_{\max l,j}}^2 . \tag{4.65}$$

The maximum of three random processes can be found by evaluating $\max(F_{\max l,j}, F_m)$.

This can be done simply by redefining the variables in equations (4.60) (4.61) (4.62) and

(4.63) then calculating the mean and variance from (4.64) and (4.65), where

$$\rho_{F_{\max l,j}F_m} = \frac{\rho_{F_l F_m}\sigma_{F_m}\Phi(\alpha) + \rho_{F_j F_m}\sigma_{F_j}\Phi(-\alpha)}{\sigma_{F_{\max l,j}}} \ . \tag{4.66}$$

Using (4.66) we can also find the correlation coefficient between the maximum of the

filtered SIRs ($F_{\max_i}$) and the fourth filtered SIR ($F_i$) as well as the unfiltered SIR ($S_i$)

$$\rho_{F_{\max i}F_i} = \frac{\rho_{F_{\max l,j}F_i}\sigma_{F_{\max l,k}}\Phi(\alpha) + \rho_{F_m Fi}\sigma_{F_m}\Phi(-\alpha)}{\sigma_{F_{\max i}}} \tag{4.67}$$

$$\rho_{F_{\max l,j(n-k)}S_i} = \frac{\rho_{Fl_{(n-k)}S_i}\sigma_{F_i}\Phi(\alpha) + \rho_{Fj_{(n-k)}S_i}\sigma_{F_j}\Phi(-\alpha)}{\sigma_{F_{\max l,j}}} \qquad (4.68)$$

$$\rho_{F_{\max i(n-k)}S_i} = \frac{\rho_{F_{\max l,j(n-k)}S_i}\sigma_{F_{\max l,k}}\Phi(\alpha) + \rho_{F_{m(n-k)}S_i}\sigma_{F_m}\Phi(-\alpha)}{\sigma_{F_{\max i}}} \,, \qquad (4.69)$$

where the bracketed subscripts indicate time, and all the unindexed variables are assumed to be at time $n$. For $FS_i = F_i - F_{\max_i}$ the mean and standard deviation are

$$M_{FS_i} = M_{F_i} - M_{F_{\max_i}} \,, \quad \sigma^2{}_{FS_i} = \sigma^2{}_{F_i} + \sigma^2{}_{F_{\max i}} - 2\rho_{F_i F_{\max i}}\sigma_{F_i}\sigma_{F_{\max_i}} \,, \qquad (4.70)$$

and the correlation coefficient between $FS_i$ and $S_i$ is

$$\rho_{FS_iS_i} = (\rho_{Fi_{(n-k)}S_i}\sigma_{F_i}\sigma_{S_i} - \rho_{F_{\max i(n-k)}S_i}\sigma_{F_{\max i}}\sigma_{S_i})/(\sigma_{FS_i}\sigma_{S_i}) \qquad (4.71)$$

To verify the validity of our approximations, Figure 12 shows a comparison between the approximated cumulative distribution function (CDF) of $FS_i$ and a simulated one.
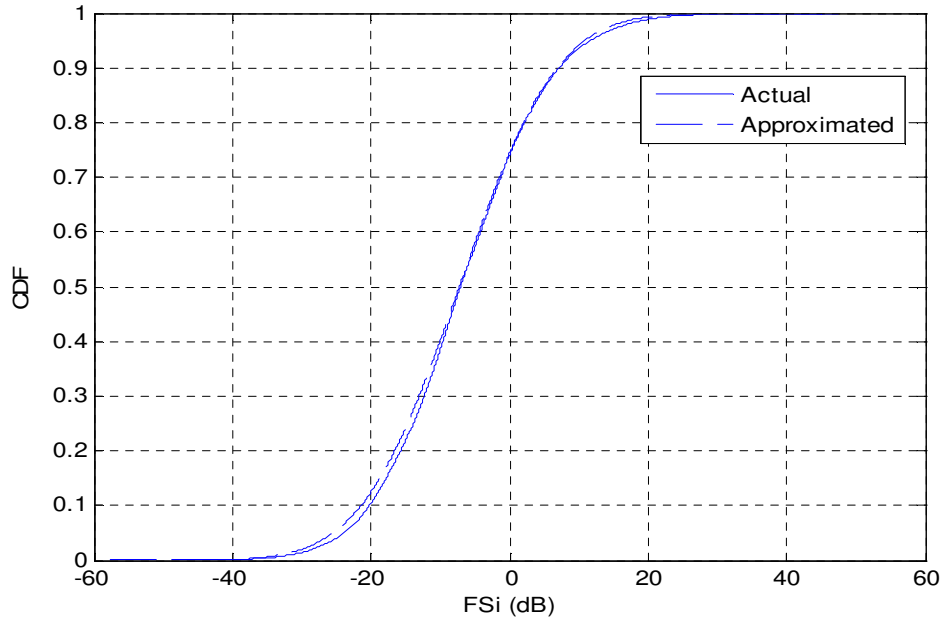


**Fig. 12. A Comparison Between the Approximated CDF and a Simulated CDF of *FSi***

Using the previous results, the SEP can now be evaluated using (4.13).

## D. SEP Numerical and Simulation Results

To confirm the accuracy of the proceeding analytical analysis over parameters of practical interest computer simulations were carried out according to the system model and handoff algorithm described in Chapter II. The communication channel was simulated as described in Chapter III. While analytical based results were obtained using (4.13). The system parameters are listed in Table II.

**Table II**
**Simulation System Parameters**

| | | |
|---|---|---|
| Carrier frequency | $f_c$ | 1.9 GHz |
| Shadow fading standard deviation | $\sigma_{Y_i}$ | 8.9 dB |
| Correlation coefficient between shadow fading components | $\rho_{Y_i Y_j}$ | 0.5 |
| Decorrelation distance for shadow fading | $d_{corr}$ | 20 m |
| First path loss constant | $K_1$ | 20 dB |
| Second path loss constant | $K_2$ | 50 dB |
| Sampling period | $T_s$ | 1.667 ms |

A comparison between numerical and simulated results using the cumulative distribution function (CDF) of the SIR received at the MS is shown in Figure 13. This CDF was obtained by varying the value of T in (4.13). The figure shows that the numerical values of the SEP match closely the simulated ones with increasing accuracy for higher MS speed. Hence, in subsequent figures only the numerical results are shown for the SEP.
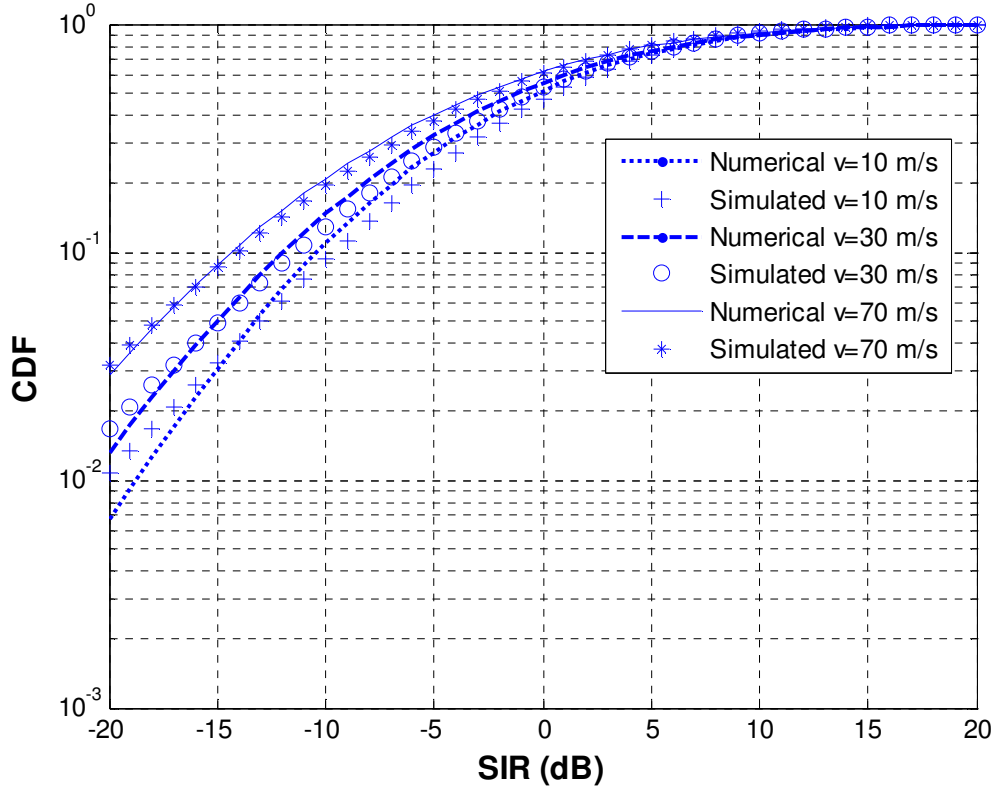


Fig. 13. Numerical and Simulated Results Comparison

The combined effects of the MS speed, the DSC length and the filter constant are captured is Figure 14.
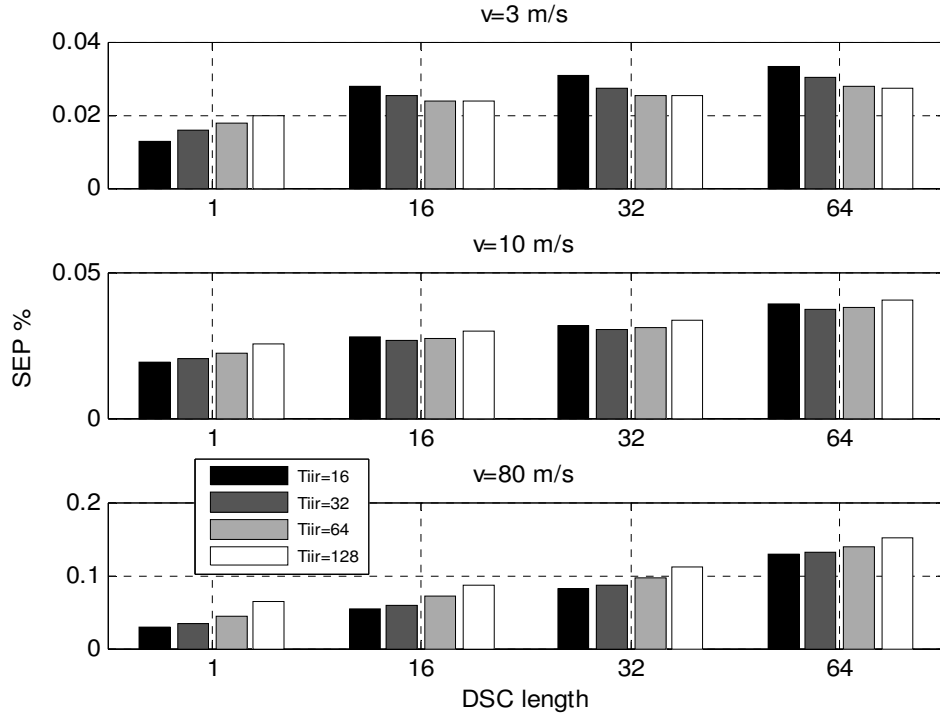
**Fig. 14. Effects of DSC Length and $T_{IIR}$ on SEP at Different MS Speeds**

As shown in Figure 14, at low speeds when the system delay is minimal (DSC length is equal to 1 slot) a lower $T_{IIR}$ means better tracking of the relatively slowly varying Rayleigh fading and hence lower SEP. As $T_{IIR}$ increases the ability of tracking the Rayleigh fading variations decreases causing the SEP to increase. But as the system introduced delay increases this close tracking of the Rayleigh fading variations becomes a disadvantage, since by the time a requested handoff is executed the SIR will have moved to a new state. Therefore, more filtering is advantageous since it filters out fast SIR changes with which the system is unable to catch up.

At medium speeds the relatively fast variations of the Rayleigh fading are filtered out. Moreover, the shadow fading is slowly changing and can be generally tracked using any of the suggested $T_{IIR}$ values. Therefore, the increase of SEP with increasing $T_{IIR}$ is caused by the increase of filtering delays. This increase is more noticeable for small DSC lengths since at large DSC lengths the system introduced delay is greater than that of the filtering and contributes more to the increase of SEP.

At higher speeds Rayleigh fading variations are still assumed to be filtered out. However shadowing variations will increase, and since smaller filter constants allow for better tracking of these variations, SEP is expected to increase when $T_{IIR}$ is increased at different DSC lengths.

# CHAPTER V

**HANDOFF PERFORMANCE - PACKET ERROR AND HANDOFF RATES**

## A. Introduction

The effects of different system parameters on the handoff performance were studied through SEP in the previous chapter. However, in packet switched systems the packet error rate (PER) is a more important measure in determining system performance. Therefore this chapter discusses the effects of the same system parameters on PER, in order to understand the insight gained about PER from SEP. Unlike SEP, PER results are obtained through simulations only. This is due to the analytical complexity imposed by packet transmission techniques employed in the Rev. A systems such as the H-ARQ.

Another important measure that must be kept in mind when analyzing handoff performance is the handoff rate, since frequent handoffs will increase the load on the network and therefore will lead for service degradation. Again only simulation results were used for the analysis of the handoff rate. Finally tradeoffs between different performance measures are presented at the end of this chapter.

## B. Packet Error Rate Simulation Technique

As mentioned in the previous chapter running link level simulations for EV-DO systems is a computationally intensive operation. However, the simulation flow for PER is affected by decisions made of whether the data in a packet was successfully decoded

or not. Therefore, in able to run slot level simulations, a technique is needed by which we can estimate the probability of decoding a packet correctly at the MS based on the SIRs associated with the pilots of the received sub-packets. An interesting technique is presented in [18], where the probability of decoding a packet correctly is calculated based on results obtained previously by running full simulations.

In general PER versus received SIR plots are obtained from link level simulations. These graphs can be then used in slot level simulations, where every time a slot is received the PER value corresponding to the received SIR of that slot is looked up from the graphs. Then based on this PER, we pseudo randomly determine if the packet was correctly decoded or not.
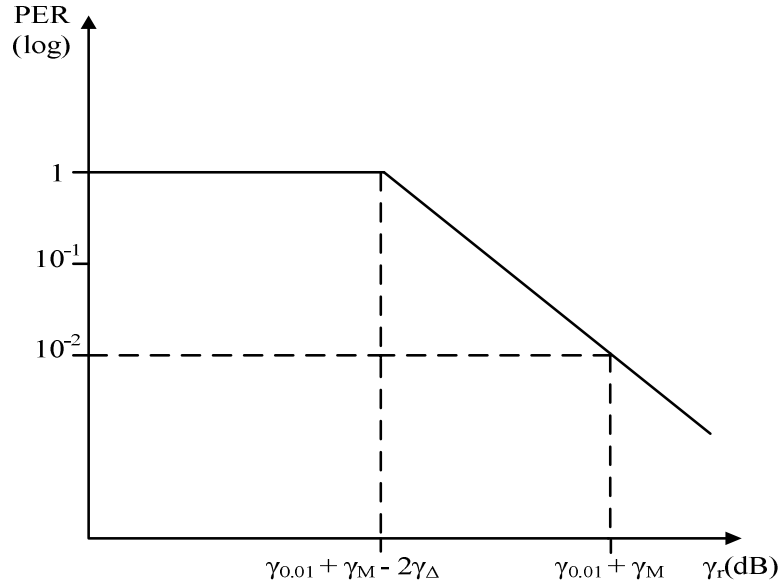


Fig. 15. PER vs. Received SIR Approximated Model

In practice, SEP versus received SIR graphs are approximated by the graph in Figure 15 , where $\gamma_r$ is the received SIR, $\gamma_{0.01}$ is the SIR required to achieve 1% PER,

$\gamma_\Delta$ is the required increase in SIR to decrease the PER by a factor of ten and $\gamma_M$ is the implementation margin which accounts for various losses, and is assumed to be equal to 2 dB [19].

From Figure 15 PER is equal to

$$PER(\gamma_r) = \begin{cases} 10^{-((\gamma_r - \gamma_{0.01} - \lambda_M + 2\gamma_\Delta)/\gamma_\Delta)}, & \gamma_r > \gamma_{0.01} + \gamma_M - 2\gamma_\Delta \\ 1 & , else \end{cases} \quad (5.1)$$

Table III carries values for $\gamma_{0.01}$ and $\gamma_\Delta$ obtained in [3]. This table only shows values for the data rate of 38.4 kbps with the packet length of 16 slots. Using this table the simulation can be run as explained below and in the flow chart in Figure 16:

- Upon the reception of a new sub-packet the linear average of all the received sub-packets' SIRs is found.

- Based on the average SIR and the number of the received sub-packets Table III is used to look up $\gamma_{0.01}$ and $\gamma_\Delta$ values.

- PER is calculated using (5.1).

- Based on the calculated PER we pseudo randomly determine whether the packet was successfully decoded or not.

- The above procedure is repeated until the packet is successfully decoded or until all the sub-packets are sent.
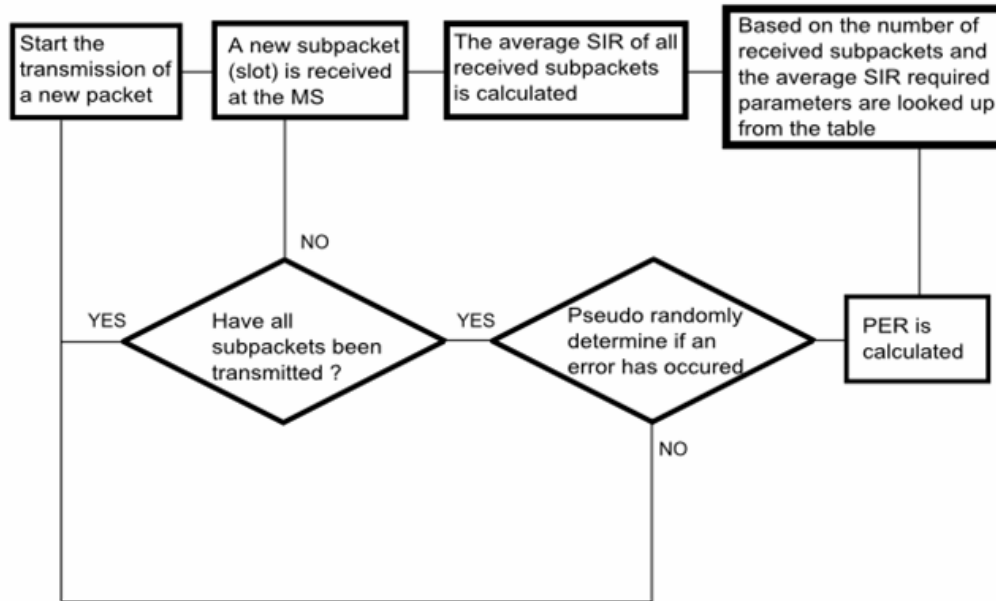
**Fig. 16. PER Simulation Flow Chart**


**Table III**
**Simulation Parameters for 38.4 kbps Data Rate**

| Sub-packet Number | Effective Data Rate | $\gamma_{0.01}r$(dB) | $\gamma_\Delta$(dB) |
|---|---|---|---|
| 1 | 614.40 | 6.7 | 0.28 |
| 2 | 307.20 | -2.9 | 0.28 |
| 3 | 204.80 | -5.3 | 0.30 |
| 4 | 153.60 | -6.9 | 0.30 |
| 5 | 122.88 | -8 | 0.30 |
| 6 | 102.40 | -8.9 | 0.30 |
| 7 | 87.77 | -9.7 | 0.28 |
| 8 | 76.80 | -10.3 | 0.29 |
| 9 | 68.27 | -10.8 | 0.29 |
| 10 | 61.44 | -11.3 | 0.29 |
| 11 | 55.85 | -11.8 | 0.29 |
| 12 | 51.20 | -12.2 | 0..30 |
| 13 | 47.26 | -12.5 | 0.30 |
| 14 | 43.89 | -12.9 | 0.31 |
| 15 | 40.96 | -13.2 | 0.30 |
| 16 | 38.40 | -13.5 | 0.45 |

Figure 17 shows the PER for 38.4 kbps data rate. The simulations were carried out as explained before. The effects of different parameters on PER are very similar to those on SEP. However since PER benefits from H-ARQ, some interesting points can be discussed.

At low speeds, it is clear that the most significant gain due to H-ARQ happens at large DSC lengths with large filter constants. This is due to the fact that at low speeds when the Rayleigh fading is still tractable by small filter constants, large filter constants are able to average fast changes in the SIR. This averaging will increase operation times at which the received SIR is good, and therefore increase the probability for most sub-packets to be transmitted at these good channel conditions. Although some sub-packets might be transmitted at the instances with bad channel conditions caused by the fast variations, their effect will be compensated for by the good sub-packets. On the other hand, at medium speeds it is shown that least achieved H-ARQ gain is at large DSC lengths with large filter constants. This is due to the fact that at these speeds where the Rayleigh fading is generally filtered out by all the suggested values of filter constants, larger filter constants introduce more filtering delays. Adding these delays to the large DSC channel delay, the MS might stay in bad channel conditions for some time before it is handed over to another BS, which will clearly increase the chance for the transmitted sub-packets to fall into bad channel conditions. Another observation that is worth noting is that the H-ARQ gain does not appear to be significant at high speeds. This is due to the fast variations of the communication channel at such speeds, which reduces the overall efficiency of the handoff algorithm in all cases.
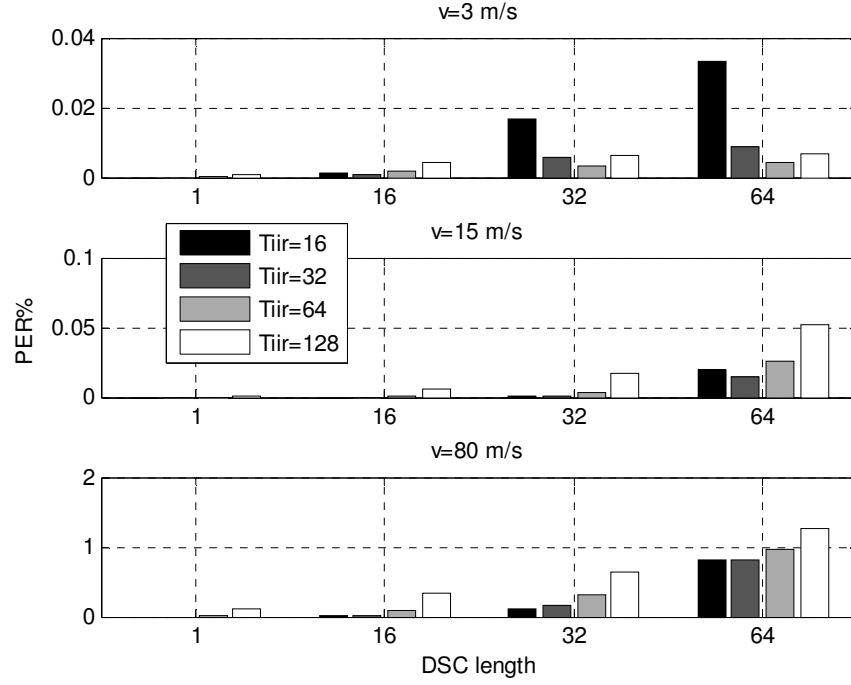
**Fig. 17. Effects of DSC Length and T$_{IIR}$ on PER at Different MS Speeds**

## C. PER with Maximal Ratio Combining

To increase data throughput receiver diversity techniques are used in EV-DO systems. In receiver diversity, multiple antennas are used at the receiver. The separation between antennas must be sufficient to assume independent fading on different paths from the transmitter to different antennas. This independence lowers the probability of experiencing simultaneous deep fades.

At the receiver different paths can be combined in different ways. Most techniques combine the paths linearly, where the outcome is a weighted sum of the different paths. The technique that achieves maximum output SINR at the receiver is

called the maximal ratio combining (MRC). In this technique every path is multiplied by a value proportional to the SINR experienced on that channel before adding it up to other paths.

Figures 18 and 19 show PER values simulated at 38.4 and 153 kbps with MRC. The SIRs received at the two antennas are assumed to be independent and identically distributed. The distribution for each antenna follows the channel model in Chapter IV. The figures show clear PER improvement achieved by MRC. Figure 19 also shows that applications that require higher data rates can be reliably served by the 1xEV-DO Rev. A systems employing seamless server selection with H-ARQ and receive diversity.
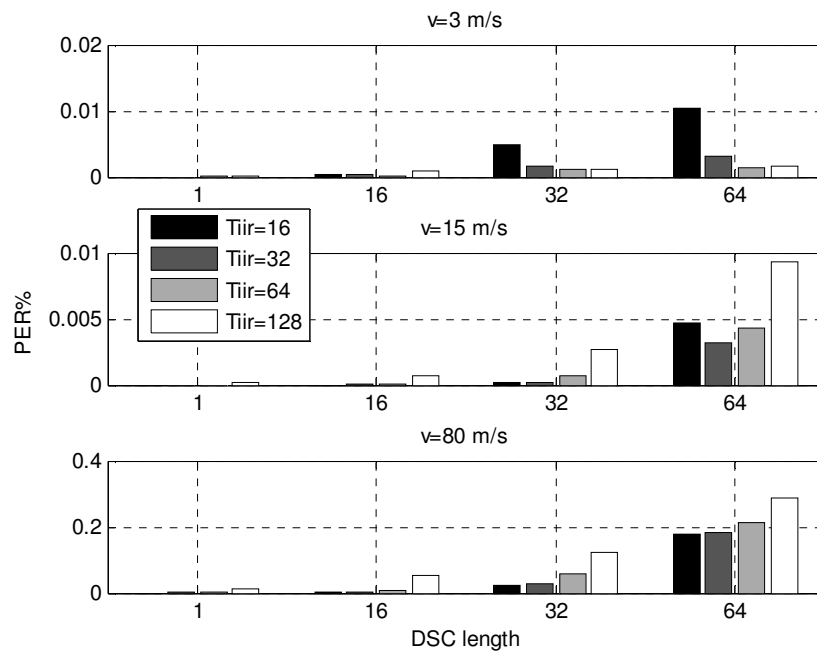


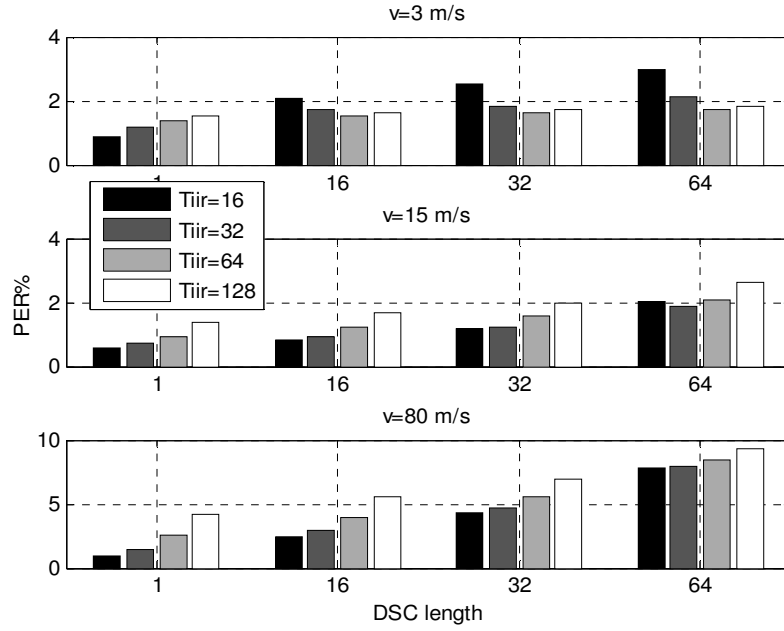Fig. 18. Effects of DSC Length and $T_{IIR}$ on PER at 38.4 kbps with MRC

**Fig. 19. Effects of DSC Length and $T_{IIR}$ on PER at 153 kbps with MRC**

## D. Handoff Rate

Another important measure of the handoff performance is the handoff rate. Although it is desirable to change the serving BS whenever the MS can achieve better PER, frequent handoffs require more system resources and increase the chance of service interruption. Figure 20 shows handoff rates for different system parameters. The figure shows that the number of handoffs decreases with an increasing $T_{IIR}$ since less fluctuation in the filtered SIRs will result in longer operating times for each BS before a handoff is initiated. Moreover it also shown that the number of handoffs slightly decreases with increasing DSC length, since recurring delays in the handoff execution will limit the number of handoffs occurring in a period of time.
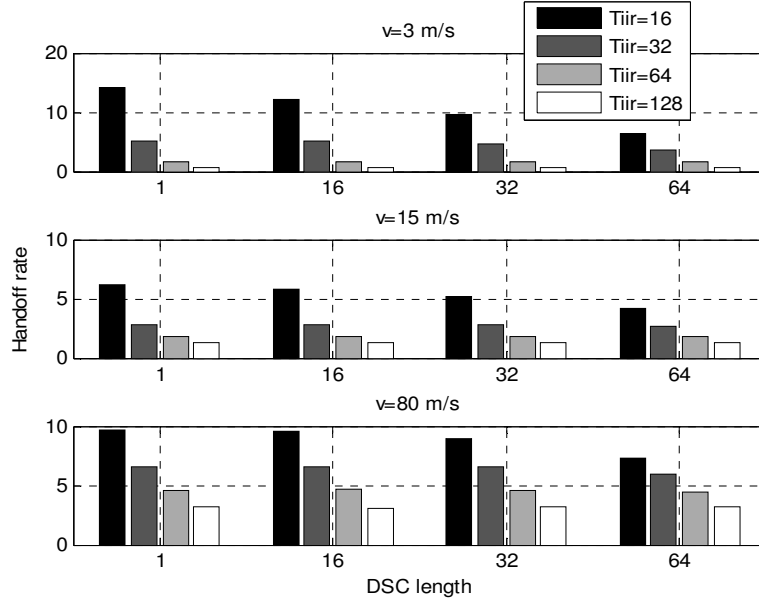
**Fig. 20. Effects of DSC Length and T$_{IIR}$ on Handoff Rate at Different MS Speeds**

Although one would expect a direct tradeoff between the handoff rate and the PER, results obtained in this chapter prove that this is not always the case. The fact that there is an introduced system delay makes large filter constants (in some cases) more desirable is terms of PER, in addition to the reduced handoff rate these constants can achieve. As a result, we observe that for practical DSC lengths, moderately large filter constants (T$_{IIR}$=64 in our case) will generally achieve better system performance for low and medium MS speeds. Moreover, their performance at high MS speeds is not significantly worse than that of smaller filter constants. Therefore, keeping in mind that handoff rates for such constants are usually low, it is generally desirable to pick large filter constants in practical systems.

## CHAPTER VI

## CONCLUSIONS AND FUTURE WORK

The performance of the handoff technique used in 1xEV-DO Rev. A systems was studied. Slot error probability (SEP) in addition to packet error rate (PER) and handoff rate were used as performance measures. An analytical approach was developed to evaluate the SEP, while PER and handoff rates were obtained using slot level simulations. Unlike previous work we adopted a multiple base station system model and accounted for correlation between shadowing components in the channel model. Moreover the effects of system parameters such as the handoff filter, DSC length and mobile station's speed on system performance measures were studied.

It was found that although absolute values of SEP and PER cannot be directly compared due the H-ARQ gain in PER, the insight gained from both of them about the system parameters effects is generally the same. It was also found that the used handoff technique in 1xEV-DO Rev. A systems can achieve acceptable performance when employing H-ARQ and receive diversity on the downlink. Finally it was found that in general moderately large filter constants are more desirable for practical DSC lengths. Moreover the results found can be used to specify system parameters based on different PER requirements and other system conditions.

The system model developed in this thesis can be further improved by including a flexible number of base stations serving a mobile station located at different distances from each base station. Packet simulations can also be enhanced to include actual data

rate requests based on the channel conditions rather than using a fixed data rate on the downlink. Finally, the analytical approach can be extended to obtain numerical results for the PER and handoff rate to replace the simulated ones.

# REFERENCES

[1]     3rd Generation Partnership Project 2 (3GPP2), "cdma2000 high rate packet data air interface specification," Technical Report C.S20024-A v1.0, Mar. 2004.

[2]     N. Bhushan, C. Lott, P. Black, R. Attar, Y. Jou, M. Fan et al., "cdma2000 1xEV-DO revision A: A physical layer and MAC layer overview," *IEEE Commun. Mag.*, vol. 44, no. 2, pp. 75- 87, Feb. 2006.

[3]     M. Yavuz, D. Paranchych, G. Wu, G. Li, and W. Krzymień, "Performance improvement of the HDR system due to hybrid ARQ," in *Proc. IEEE Vehic. Tech. Conf.*, Atlantic City, NJ, Oct. 2001, vol. 4, pp. 2192-2196.

[4]     C. Patel, M. Yavuz, and Y. Tokgoz, "Handoff performance analysis for 1xEV-DO Rev. A systems," in *Proc. IEEE Int. Conf. Commun.*, Istanbul, Turkey, Jun. 2006, vol. 11, pp. 4924-4929.

[5]     M. Gudmundson, "Correlation model for shadow fading in mobile radio systems", *IEE Elec. Lett.*, vol. 27, no. 23, Nov. 1991.

[6]     3GPP2 TSG-C WG3, "1xEV-DO evaluation methodology," TSG-C Contribution C30-20031002-004, Oct. 2004.

[7]     R.H. Clarke, "A statistical theory of mobile-radio reception," *Bell Syst. Tech. J.*, vol. 47, pp. 957-1000, Jul.-Aug. 1968.

[8]     M. Patzold, U. Killat, F. Laue, and Y. Li, "On the statistical properties of deterministic simulation models for mobile fading channels," *IEEE Trans. Veh. Technol.*, vol. 47, pp. 254-269, no. 1, Feb. 1998

[9]   S. Das, W. M. MacDonald, and H. Viswanathan, "Sensitivity analysis of handoff algorithms on CDMA forward link," *IEEE Trans. Veh. Technol.*, vol. 54, no. 1, pp. 272-285, Jan. 2005.

[10]  M. D. Turkmani, "Probability of error for M-branch macroscopic selection diversity," in *Proc. Inst. Elect. Eng-I Commun., Speech and Visions*, vol. 139, Feb. 1992, pp. 71-78.

[11]  A.M. Law, and W.D. Kelton, *Simulation Modeling and Analysis*, 4th Edition, Boston, MA: Mc.Graw Hill, 2007.

[12]  S. Schwratz and Y. S. Yeh "On the distribution function and moments of power sums with lognormal components," *Bell Syst. Tech. J.*, vol. 61, pp.1441-1462, Sep. 1982.

[13]  A. Abu-Dayya and N. C. Beaulieu, "Outage probabilities in the presence of correlated lognormal interferers," *IEEE Trans. Veh. Technol.*, vol. 43, pp. 164–173, Feb. 1994.

[14]  A. Ligeti, "Outage probability in the presence of correlated lognormal useful and interfering components," *IEEE Commun. Lett.*, vol. 4, pp. 15-17, Jan 2000.

[15]  F. Graziosi and F. Santucci, "A general correlation model for shadow fading in mobile radio systems," *IEEE Commun. Lett.*, vol. 3, pp. 102–104, Mar. 2002.

[16]  C. Fischione, F. Graziosi, and F. Santucci, "Approximation of a sum of onoff lognormal processes with wireless applications," in *Proc. of IEEE Int. Conf. Commun.*, Paris, France, Jun. 2004, vol. 1, pp. 306-310.

[17] J.G. Proakis and D.G. Manolakis, *Digital Signal Processing: Principles, Algorithms, and Applications*, 3rd ed. Englewood Cliffs, NJ: Prentice-Hall, 1996.

[18] D.W. Paranchych and M. Yavuz "A method for outer loop rate control in high data rate wireless networks," in *Proc. IEEE Veh. Technol. Conf.*, Vancouver, Canada, Sep. 2002, vol. 3, pp. 1701-1705.

[19] P. Bender, P. Black, M. Grob, R. Padovani, N. Sindhushayana, and A. Viterbi, "CDMA/HDR: A bandwidth efficient high-speed wireless data service for nomadic users," *IEEE Commun. Mag.*, vol. 39, no. 7, pp. 70-77, Jul. 2000.

**VITA**

Name:              Maher Al-Shoukairi

Address:           214 Zachry Engineering Center, College Station, Texas 77843

Email Address:     maher@ece.tamu.edu

Education:         B.S., Electrical Engineering, University of Jordan, Jordan, 2005
                   M.S., Electrical Engineering, Texas A&M University, 2008